RIVERSIDE RESEARCH INSTITUTE

TECHNICAL REPORT T-1/364-3-65

PHOTOCOUNTING IMAGE TRACKING OF FLUCTUATING TARGETS

by Marek Elbaum

RIVERSIDE RESEARCH INSTITUTE

80 West End Avenue / New York, New York 10023 / (212) 873-4000

February 1977

TECHNICAL REPORT T-1/364-3-65

PHOTOCOUNTING IMAGE TRACKING OF FLUCTUATING TARGETS

by Marek Elbaum

Sponsored by

Defense Advanced Research Projects Agency
Department of Defense
ARPA Order Nr. 2281, Amd. 14

Monitored by

U. S. Army
Missile Research and Development Command
Redstone Arsenal, AL 35809

Contract No. DAAK40-76-C-0500
Technical Requirement Nr. 6004

AUTHORIZATION

The research described in this report was performed at Riverside Research Institute. The report was written by Marek Elbaum.

This research project was supported by the Defense Advanced Research Projects Agency of the Department of Defense and administered by the U.S. Army Missile Research and Development Command under contract number DAAK40-76-C-0500.

Submitted by

Marek Elbaum

Marek Elbaum
Member, Research Staff

Approved by:

Marvin King

Marvin King
Research Director

ACKNOWLEDGEMENT

The author expresses his appreciation to Prof. P. Diament of Columbia University for his deep and thorough criticisms of the original manuscript.

The author is grateful to Dr. M. King, Dr. K. S. Miller, W. Edelson, and Dr. M. Greenebaum for valuable discussions.

ABSTRACT

A theory of estimation of angular position and other attributes of optically rough and smooth targets with a monopulse laser radar is developed. It applies to systems deriving information about the target position by sensing its image with an array of noncoherent detectors. The theory develops quantitative formulations of the fundamental limitations imposed upon measurement accuracy by the shot noise arising from both the target return and the background radiation, by the detector dark current, and by the random fluctuations of the target cross section.

CONTENTS

I. INTRODUCTION

The potential of considerably higher accuracy than that of microwave radar motivates interest in employing laser radar for angle tracking. With the recent advent of high-power lasers, angle-tracking laser radars are particularly attractive for space-borne applications where, due to the absence of atmospheric turbulence, the potential for high accuracy, which results primarily from employing short wavelengths, can be used to full advantage. High-accuracy tracking used for precision pointing of a communication laser beam from one satellite to another distant satellite promotes efficient use of laser energy in the communication link. It has also been pointed out that precise knowledge of the relative positions of two spacecraft performing a rendezvous maneuver is difficult and often impractical to obtain from ground-based radars; accurate laser radars located on board a spacecraft could serve as accurate guidance aids.

In an angle-tracking system, a sequence of direct measurements of target position is fed into a tracking filter, which can produce refined estimates of past, present and future target position. Generally, the accuracy of the refined estimate is proportional to the accuracy of direct measurements, so that

schemes for improving measurement accuracy are potentially of great significance.

Relative to the volume of research on angular tracking of unresolvable targets with microwave radars, initiated during World War II, or on passive tracking of resolved targets reported more recently in the infrared and visible regions, very few papers have been published bearing on the problem dealt with herein.

When applied to tracking in the optical region, such well-known and established microwave radar tracking techniques as amplitude and phase monopulse need to be reassessed and extended to cover at least two new aspects. First, the classical wave description used successfully in microwave radars is not adequate: since the energy of a single optical photon is so much greater than that of a microwave photon, there are far fewer photons arriving at the receiver in any case of practical interest. One cannot assume, even in principle, that there exists a noise-free limit in which it is possible to find the position of an object exactly. The position estimator of an optical object is always subject to error which, in the most optimistic case, is quantum-noise limited. Second, the theory of angular position estimators of nonresolvable, point-type targets must be extended: the fine resolution of optical imaging systems allows one to distinguish various features on the object, and tracking of resolvable targets must be considered.

Furthermore, microwave-radar design literature offers little or no information for tracking targets illuminated with partially coherent radiation, as might be the case where efficient multi-line HF lasers are used, or for the systems using direct detection.

This thesis addresses the issue of target angular position (TAP) estimation with a pulsed laser radar. The TAP estimates are obtained from the targets' images. The imaging system receives ligth from both the target that has been illuminated with the laser beam provided for tracking and from uniform, noncoherent background radiation. This light is imaged onto the detector array, which converts the photon flow into an image photocounting distribution (IPD), the electrical signal used by the image processor. The purpose of the image processor is to estimate accurately the image position for each received pulse.

The thesis analyzes several image processors based on the derived estimators of the TAP. Their accuracy is discussed and compared. In this comparison, the beam-splitting ratio, which is understood here as the factor by which the processor accuracy can be improved above the diffraction-limited resolution of the imaging system, is used as the figure of merit. In the next section the scope of the thesis is outlined. The results are summarized in the last section of this chapter.

1.1 Outline

The analytical results presented in this thesis have been developed in four major steps:

a. The semiclassical photon-counting theory was used to obtain a model for the Image Photoelectron-Counting Profiles produced at the array output in response to the irradiance distribution at the image plane. This irradiance was assumed to be a sum of two terms, representing the target image and a uniform, noncoherent background. A mathematical model for the image irradiance that takes into account the coherence of illumination, target surface roughness, and the illuminator-target-imaging system geometry was developed. Mandel's transformation was used to relate this model to the statistical properties of the image photoelectron-counting profile.

b. The faithfulness with which the image photocounting distribution provides knowledge about the image irradiance was addressed by calculating the signal-to-noise ratio at the output of the individual detectors in the array. A general expression for the SNR was obtained as a function of the relevant target and system parameters.

c. For the targets much smaller than the diffraction-limited resolution of the imaging system, their angular position was estimated, based on image sensing by a four-quadrant detector. The lower Cramér-Rao bounds were established for the estimates. The maximum likelihood estimates of the angular

position were derived for optically rough and smooth targets and their performance compared with the theoretical limits.

d. The problem of estimation of angular position of extended targets, well resolved by the pupil aperture, was addressed by considering the properties of the image centroid estimator. The mean and variance of this estimator were expressed in terms of the covariance matrix of the photoelectrons at the outputs of the detectors that form the elements of the large array. The properties of this matrix were discussed for optically rough and smooth targets. The variance of the centroid estimator was obtained as a function of relevant target and system parameters.

1.2 Summary of Results

The problems of TAP estimation with monopulse laser radars has been analyzed for systems that derive the desired information out of a single pulse from the target's image, which is sensed with an array of noncoherent detectors.

In Chapter II, a general expression for the signal-to-noise ratio (SNR) at the output of an individual detector in the array is obtained as a function of the coherence of the illuminating light, the object surface roughness, the width of the telescope point spread function, and the aperture and integration time of the detector. The expression is evaluated for several limiting cases of coherence of illumination and of object surface roughness. The expression indicates that, for

increasing signal levels, the SNR is limited first by background noise, then by signal shot noise, and ultimately by the target fading. The target fading manifests itself as the random fluctuations of the laser radar target cross section.

The fading contrast involves stochastic, spatial, and temporal averaging of the second moment of the image irradiance, or the degree of coherence, which propagates from the rough target to the image plane. The roughness enters by way of the joint characteristic function of the surface statistics. The expressions obtained for the fading contrast reveal quantitatively the efficiency of various means for improving fading-limited SNR, by temporal averaging, by spatial averaging, or by increased bandwidth of illumination. Plots of the SNR against bandwidth for various roughness scales, and against signal strength for various noise and fading levels, are presented and it is shown that the SNR can be improved at the expense of spatial resolution.

In Chapter III, the angular position of a target unresolved by the imaging system is estimated by measuring the location of the target's photocounting image by means of a noncoherent four-quadrant detector. The choice of estimator depends on the statistics of the photocounts, which reflect those of the energy deposited on the detectors by the laser field returned from the target. For an optically rough target, this is a spatio-temporal complex Gaussian process, producing photo-

electrons that obey a negative binomial distribution with M degrees of freedom. The limitations imposed by target fading and by signal and background shot and dark current noise on the accuracy of the estimate are investigated. The theoretical limits given by the Cramér-Rao lower bounds for the standard deviations of the estimates are derived for fading and nonfading targets. For several cases it is shown that the lower bounds are given by the beam-splitting formula; i.e., that the standard deviations are proportional to the diffraction-limited angular resolution of the imaging telescope and inversely proportional to the SNR, where the noise includes the shot noise generated by the target and background radiation and dark current, and do not depend on the target fading.

Maximum likelihood estimates are derived for fading and nonfading targets and their means and standard deviations are evaluated. All these estimates share the following properties:

a. They depend on the familiar monopulse ratio which, for the photocounting problem is given by the ratio of the difference of the total number of photocounts at the detector outputs to their sum. This normalization makes the angular measurement independent of the target range and significantly reduces the impact of target fading on its accuracy.

b. They are biased. For nonfluctuating targets, the bias decreases exponentially with the signal and background noise. For fading targets the bias decreases monotonically

with the signal at a rate that depends on the number of degrees of freedom in the image radiation.

c. The standard deviations of the estimates approach the theoretical Cramér-Rao limits for unbiased estimates when the signals are large enough to make the MLEs unbiased.

The last chapter discusses TAP and target size estimation of extended targets. The image centroid estimator, and that for its second moment, are obtained by processing the image photocounting distribution at the output of the multielement detector array sensor. The expressions for the means and covariance matrices of the estimators are derived and discussed.

a. Both estimators are biased; the biases are inversely proportional to the square of the overall SNR at the sensor output.

b. The rms errors are inversely proportional to the SNR.

c. The biases and rms errors of the estimators depend on the detection matrix, comprised of the covariances between the photocounts at the outputs of pairs of detectors in the array. The detection matrix becomes diagonal, giving the variances of the photocounts at the individual detector outputs, for either nonfluctuating targets or noncoherent illumination, or also for fluctuating targets generating Gaussian image fields, if the detectors sample them at the Nyquist rate.

d. For diagonal detection matrices and nonfluctuating targets, the bias and rms error of the centroid estimator decrease with increasing laser power; for flutuating targets they cannot be decreased below the limit imposed by laser-speckle noise. This limitation improves with the number of degrees of freedom in the image, which depends on the diffraction-limited resolution of the imaging system.

II. SNR IN PHOTOCOUNTING IMAGES OF ROUGH OBJECTS IN PARTIALLY COHERENT LIGHT

Image irradiance distributions from objects illuminated with partially coherent, quasi-monochromatic light, viewed against a spatially uniform background and received with a photosensitive detector are analyzed. A general expression for the signal-to-noise ratio at the detector output is obtained as a function of the coherence of the illuminating light, the object surface roughness, the width of the telescope point spread function, and the aperture and integration time of the detector. The expression is evaluated for several limiting cases of coherence of illumination and of object surface roughness.

Published in Appl. Optics, 15, 2268-2275 (1976) with P. Diament.

2.1 INTRODUCTION

Communication theory shows that the rate of transmission of information is limited by two basic system properties: the bandwidth through which the signal information passes, and the noise inherently present in all systems. Analysis of the trade-off between signal-to-noise ratio (SNR) and bandwidth is an important part of the evaluation of communication systems.

The information conveyed about an object by an imaging system can be encoded both in time and in space. For systems employing direct detection, it is the spatial correspondence between the irradiances at the objects and at their images that is of primary interest. In systems such as laser tracking radars, estimates of the position of laser-illuminated objects are derived from their images. If the images are to be observed with an array of detectors, the SNR analysis can help decide whether the array should consist of many detectors with small apertures (high complexity, high resolution) or fewer detectors with larger apertures (less complexity, lower resolution).

The generality of the system to be considered is suggested in Fig. 1. The object is illuminated with quasi-monochromatic, partially coherent light. The surface of the object has a height profile $z(\underline{x}_o)$ and a reflection coefficient $\eta(\underline{x}_o)$ that are stochastic processes. We take $z(\underline{x}_o)$ to be a stationary, Gaussian, zero-mean process. The widths of the correlation coefficients of the two processes, ρ_z and ρ_η, are assumed sufficiently large with respect to the wavelength to justify

use of the scalar theory of diffraction. As a result of scattering from the object surface, the transverse coherence originally present in the illuminating field is modified, so that the field leaving the object becomes random in time and in space. The imaging telescope further modifies the transverse coherence of the field at the image plane. The total image-plane irradiance distribution, consisting of the sum of object and background irradiance contributions, is sensed with a photodetector, which imposes additional noise processes associated with photon counting and dark current. We seek the SNR at the output for an object illuminated with partially coherent, quasi-monochromatic radiation, in the presence of uniform, thermal background radiation.

The imaging of partially coherent objects was first studied by Hopkins[1] and, more recently, by Ichioka[2]. Enloe[3], Lowenthal and Arsenault[4], and Dainty[5] have analyzed the statistical properties of the images of coherently-illuminated diffuse objects. They found that the noise-like, speckled structure of the image has a mean square intensity equal to the square of the mean intensity. Enloe, identifying the signal with the expected value of the fluctuations of the image irradiance distribution and the noise with their standard deviation, suggested that the SNR can be improved at the expense of the spatial resolution of the imaging system. Elbaum, Greenebaum and King[6], and George and Jain[7] have studied the improvement in SNR when multi-frequency illumination is employed instead of nearly-monochromatic light. The effects of surface roughness on the statistical distribution of image speckle intensity

have been measured by Fujii and Asakura[8].

Goodman[9] was the first to discuss the properties of laser speckle patterns as they affect the performance of optical radars. Treating the field scattered from a coherently illuminated object as a complex Gaussian process over space, Goodman applied Mandel's theory of photodetection to compute the resulting photocounting statistics. This paper combines Wolf's[10] theory of propagation of coherence and Mandel's[11] photodetection theory to obtain generalized expressions for SNR.

The expressions obtained extend the one derived by Bures[12] for measuring degeneracy of light, are not restricted to Gaussian light and include background and dark current noises. When specialized to Gaussian linearly polarized light, they reveal explicitly the dependence of the SNR on coherence of illumination, object surface roughness, coherent point spread function, aperture of detector, and integration time. Although interest is directed to irradiances at the image plane, most of the results obtained in this paper can be adapted to apply to irradiances at any plane.

In the next section, the semiclassical theory of photodetection is employed to obtain a general formula for the SNR at the output of the detector. In Section 2.3 the SNR is discussed for large signal levels, where the limitations are imposed by the random fading of the field across the detector. Several limiting cases of illumination coherence and surface roughness are considered. Section 2.4 treats the SNR for small signal levels, where signal-shot-noise and background and dark

current noise must be included. The tradeoffs between SNR and spatial resolution are considered in Section 2.5.

2.2 General Expression for Signal-to Noise Ratio

We seek to estimate significant features of the irradiance at the object from observations of the number of photocounts at the output of a detector that senses the image irradiance distribution. We consider a photosensitive detector with an aperture A illuminated by the image irradiance $I(\underline{x}_i, t)$. In general the total number of counts n_T observed at the output of the detector during some integration time T includes signal and background photoelectrons, n_S, n_B, and dark current electrons, n_D; i.e.,

$$n_T = n_S + n_B + n_D \,. \tag{1}$$

The first two terms are generated by the energy deposited on the detector by the electromagnetic fields that arrive from the object and from the background. The third term is generated internally in the detector and depends only on the detector quality. We associate the signal, S, with the expected value, $\langle n_s \rangle$. The noise level, N, may be defined as the standard deviation of the counts, σ_T, which measures the random fluctuations at the detector output. Since the three terms in (1) are generated by independent physical mechanisms and may be treated as mutually independent stochastic processes, the variances of the signal, background, and dark current counts simply add, so that the noise level is

$$N = \sigma_T = (\sigma_S^2 + \sigma_B^2 + \sigma_D^2)^{1/2}. \tag{2}$$

The semiclassical theory of photoemission developed by Mandel[11] treats the number of photoelectrons, n, resulting from the total electromagnetic field energy, $W=W_T$, deposited on the detector, as a nonhomogeneous Poisson process with mean and variance given in terms of those of W by

$$\langle n \rangle = \alpha \langle W \rangle \tag{3}$$

and

$$\sigma_n^2 = \langle n \rangle + \alpha^2 \sigma_W^2 \quad . \tag{4}$$

The energy is related to the irradiance by

$$W = \int_T dt \int_A d^2x_i \, I(\underset{\sim}{x}_i, t) \tag{5}$$

and the coefficient of proportionality, $\alpha = \xi / h\bar{\nu}$, involves the quantum efficiency of the detector, ξ, and the average frequency of the field, $\bar{\nu}$; h is Planck's constant. The first term in (4) is the variance of the photoelectron count associated with the photoelectric effect and represents the intrinsic fluctuations in the detection process. The second term, which depends on the fluctuations of W, represents an excess fluctuation of counts due to bunching of photoelectrons. The process is thus doubly stochastic.

When the integration time, T, is much larger than the coherence time of the background radiation, the temporal fluctuations are averaged out and the bunching effect for the background radiation is absent; i.e., $\sigma_B^2 = \langle n_B \rangle$. Similarly, the dark count is assumed to be distributed according to Poisson statistics[13], with parameter $\langle n_D \rangle$, so that

$\sigma_D^2 = \langle n_D \rangle$. It follows that the SNR can be written as

$$\text{SNR} = \frac{\langle n_S \rangle}{\sigma_T} = \frac{\langle n_S \rangle}{\left[\langle n_S \rangle + \alpha^2 \sigma_W^2 + \langle n_N \rangle\right]^{1/2}} \tag{6}$$

where $\langle n_N \rangle = \langle n_B \rangle + \langle n_D \rangle$, and W is the energy deposited on the detector by the field from only the object. To analyze the relative strengths of the three contributors to the noise, a modified version of (6), using (3), is useful

$$\text{SNR} = \left(\frac{1}{\langle n_S \rangle} + \frac{\sigma_W^2}{\langle W \rangle^2} + \frac{\langle n_N \rangle}{\langle n_S \rangle^2} \right)^{-1/2} . \tag{7}$$

The second term depends on the spatio-temporal properties of $I(\underline{x}_i, t)$ modified by the temporal and spatial integration at the detector.

For the special case of an aperture and integration time small with respect to the coherence time, the energy becomes $W = IAT$ and the middle ratio can be written as $\sigma_I^2 / \langle I \rangle^2$. In the theory of laser speckle patterns[3-9], the ratio $C_I = \sigma_I / \langle I \rangle$ is treated as a measure of the contrast of the spatially random pattern. $C_I = 1$ for Gaussian light. It is convenient to extend the notion of the contrast of I to that of the energy W received by the detector. The contrast of W, $C_W = \sigma_W / \langle W \rangle$, generalizes C_I and can be interpreted as the contrast of the measured fading.

The general formula for the signal-to-noise ratio, rewritten now as

$$SNR = \frac{\langle n_S \rangle^{1/2}}{[1 + C_W^2 \langle n_S \rangle + \frac{\langle n_N \rangle}{\langle n_S \rangle}]^{1/2}} \quad , \tag{8}$$

yields some important limiting cases. For large signals ($n_S >> n_N, C_W^{-2}$) the SNR is signal-fading-limited and equal to the inverse of the contrast: $SNR = C_W^{-1}$. For noiseless W, ($C_W = 0$), the SNR depends only on signal-shot-noise and background and dark current noises: $SNR = \langle n_S \rangle / [\langle n_S \rangle + \langle n_N \rangle]^{1/2}$. For background noise larger than the signal, ($n_N >> n_S$), the SNR is background-noise-limited: $SNR = \langle n_S \rangle / \langle n_N \rangle^{1/2}$.

2.3 Fading-Limited SNR

This section discusses the fading contrast, C_W, for complex Gaussian fields. We first treat fading contrast in terms of the temporal properties of the illuminating field and the illuminator-object-imaging system geometry, then apply the results to computations of fading contrast for optically rough and smooth surfaces and for limiting values of integration time and detector aperture. Several practically important cases of illumination are considered: case (a) treats cross-spectrally pure light; case (b) addresses monochromatic illumination; case (c) considers the effects of polychromatic illumination on the contrast.

To gain a qualitative insight into computations of contrast of fading, consider a laser-generated field $V^{(1)}$ at the object, characterized by some coherence area and time, A_1 and T_1. The field leaving the object, $V^{(2)}$, has coherence area and time, A_2 and T_2. If the target is stationary

with respect to the illuminating beam, the coherence times of $V^{(2)}$ and $V^{(1)}$ may be assumed equal. However, the transverse coherence, whose area A_1 is assumed to be larger than the object's dimensions[14], can be modified by the object surface roughness, or even destroyed completely. Propagation of the field $V^{(2)}$ in space and the spatial filtering imposed by the imaging telescope lead to a further-modified coherence area and time of the image field, $V^{(3)}$. For spatially incoherent objects, for example, the coherence area A_3 is that of the diffraction-limited resolution cell at the image plane[3, 4]. The coherence time T_3 is equal to T_2 if the maximum differential time delay in propagating along different optical paths from the object points to the image plane is much smaller than T_2; otherwise T_3 is smaller than T_2.

2.3.1 General Theory

Computation of the fading contrast is a difficult task in general; it depends on the covariance function of the image irradiance and therefore requires evaluation of the fourth moment of the field at the image plane:

$$C_W^2 = \frac{\int dt_1 \int dt_2 \int d^2x_{i1} \int d^2x_{i1} \quad \mathrm{cov}\{I_1, I_2\}}{\int dt_1 \int dt_2 \int d^2x_{i1} \int d^2x_{i2} \langle I_1 \rangle \langle I_2 \rangle} \quad . \tag{9}$$

The integrations in time and space are over T and A respectively, I_1, I_2 are irradiances at $\underset{\sim}{x}_{i1}$, t_1 and $\underset{\sim}{x}_{i2}$, t_2, and

$$\mathrm{cov}\{I_1, I_2\} = \langle I_1 \; I_2 \rangle - \langle I_1 \rangle \langle I_2 \rangle \quad . \tag{10}$$

For complex Gaussian fields,[15, 16] the covariance of the irradiance

can be expressed in terms of the degree of coherence, $\gamma_{12}(\Delta t)$.

$$\text{cov}\{I_1, I_2\} = |\gamma_{12}(t_1, t_2)|^2 \langle I_1 \rangle \langle I_2 \rangle, \tag{11}$$

where

$$\gamma_{12}(t_1, t_2) = \langle V^{(3)}(\underset{\sim}{x}_{i1}, t_1)\, V^{(3)*}(\underset{\sim}{x}_{i2}, t_2)\rangle / (\langle I_1 \rangle \langle I_2 \rangle)^{1/2}. \tag{12}$$

When such fields are stationary and linearly polarized, the fading contrast reduces to

$$C_W^2 = A^{-2} T^{-2} \int dt_1 \int dt_2 \int d^2x_{i1} \int d^2x_{i2} \, |\gamma_{12}(\Delta t)|^2 \tag{13}$$

where $\Delta t = |t_1 - t_2|$. The reciprocal of this is often interpreted as the number of degrees of freedom in linearly polarized light[12].

Using Wolf's[10] theory of propagation of the coherence function, the degree of coherence at the image plane, $\gamma_{12}(\Delta t)$, can be expressed[26] in terms of the degree of coherence of the field leaving the object, $\gamma_{12}^{(2)}(\Delta t)$:

$$\gamma_{12}(\Delta t) = F_{12} * \langle \gamma_{12}^{(2)}(\Delta t + R/c)\rangle \ , \tag{14}$$

in which the deterministic transfer operator F_{12} is applied to the expected value of the propagated $\gamma_{12}^{(2)}(\Delta t)$. $R(\underset{\sim}{x}_{o1}, \underset{\sim}{x}_{o2}, \underset{\sim}{x}_{i1}, \underset{\sim}{x}_{i2})/c$ is the differential time delay in propagating along different optical paths, one from $\underset{\sim}{x}_{o1}$ to $\underset{\sim}{x}_{i1}$ and another from $\underset{\sim}{x}_{o2}$ to $\underset{\sim}{x}_{i2}$. The expectation is taken with respect to realizations of R, which depends on random variable z, and of the random reflection coefficient, η. This operation is dictated here by defining the coherence to apply to ensembles of both light sources and scattering surfaces.

If the differential time delay R/c is much smaller than the coherence time T_2, then $\langle \gamma_{12}^{(2)}(\Delta t + R/c)\rangle$ can be factored into

$$\langle \gamma_{12}^{(2)}(\Delta t + R/c)\rangle = \langle \gamma_{12}^{(2)}(\Delta t)\rangle \langle \exp(j2\pi \bar{\nu} R/c)\rangle . \tag{15}$$

The first factor is the expectation of the degree of coherence of the emergent field at the object, with respect to the random reflection coefficient. It may be expressed as the product of the degree of coherence of the illuminating field, $\gamma_{12}^{(1)}(\Delta t)$, and the mutual correlation coefficient of η at two object points, $\rho_\eta(\Delta \underset{\sim}{x})$. In the second factor, the path-length difference R can be decomposed into the sum of a deterministic part, $D(\theta)$, and a random part, $Z(\theta)$. The former depends on the angle of incidence θ of the illumination and on the optical path lengths between points on the median scattering surface and the image plane. The random part,

$$Z(\theta) = [z(\underset{\sim}{x}_{o1}) - z(\underset{\sim}{x}_{o2})](1 + \cos\theta), \tag{16}$$

involves the spatial structure of the surface roughness, $z(\underset{\sim}{x}_o)$, and the obliquity factor.

The factor due to the surface roughness is expressible as

$$\langle \exp(j2\pi \bar{\nu}\, Z/c)\rangle = \phi(k', -k'), \tag{17}$$

where $\phi(k_1, k_2) = \langle \exp[j(k_1 z_1 + k_2 z_2)]\rangle$ is the joint characteristic function of $z(\underset{\sim}{x}_{o1})$ and $z(\underset{\sim}{x}_{o2})$ and $k' = 2\pi(\bar{\nu}/c)(1+\cos\theta)$. The remaining factor combines with the deterministic impulse response in a convolution that accounts for all the geometrical effects, including the telescope aperture, leaving

$$\gamma_{12}(\Delta t) = \int d^2x_{o1} \int d^2x_{o2}\, H_{12}(\underset{\sim}{x}_{o1}, \underset{\sim}{x}_{o2})\, \phi(k', -k')\, \rho_\eta(\Delta \underset{\sim}{x}_o)\, \gamma_{12}^{(1)}(\Delta t), \tag{18}$$

where H_{12} is the impulse response in the absence of surface roughness

and for uniform reflection properties. The consequences for several cases of interest can now be examined.

a. Cross-Spectrally Pure Illumination

If in addition to $R/c << T_2 = T$, the spectral density of the light at the target is uniform, the last factor in (18) is reducible to the product of the spatial and temporal degrees of coherence $\gamma_{12}^{(1)}(0)$ and $\gamma_{11}^{(1)}(\Delta t)$[17]. Thus, for Gaussian fields satisfying the condition of cross spectral purity, the degree of coherence at the image plane becomes $\gamma_{12}(\Delta t) = \gamma_{12}(0)\,\gamma_{11}(\Delta t)$ where

$$\gamma_{12}(0) = \int d^2x_{o1} \int d^2x_{o2}\, H_{12}(\underset{\sim}{x}_{o1}, \underset{\sim}{x}_{o2})\phi(k', -k')\rho_\eta(\Delta\underset{\sim}{x}_o)\,\gamma_{12}^{(1)}(0) \qquad (19)$$

and $\gamma_{11}(\Delta t) = \gamma_{11}^{(1)}(\Delta t)$. This indicates that the degree of spatial coherence at the image plane results from propagation of the transverse coherence of the illumination, modified by the object surface structure. In particular for $\gamma_{12}^{(1)} = 1$, $\gamma_{12}(0)$ at the image depends only on object surface structure and on the coherent point spread function of the system. On the other hand the temporal degree of coherence remains unchanged provided that the illuminator, object, and receiver do not move with respect to each other during the measurement. For this case the square of the fading contrast, C_a, is

$$C_a^2 = (T^{-2}\int dt_1 \int dt_2 \,|\gamma_{11}^{(1)}(\Delta t)|^2)(A^{-2}\int d^2x_{i1} \int d^2x_{i2}\,|\gamma_{12}|^2) \qquad (20)$$

b. Monochromatic Illumination

Laser illumination is often idealized as fully monochromatic radiation:

$$V^{(1)}(\underset{\sim}{x}_{o1}, t) = U(\underset{\sim}{x}_o) \exp[-j2\pi \nu_o t]. \tag{21}$$

It follows that the degree of coherence, $\gamma_{12}^{(1)}(\Delta t)$, is given by:

$$\gamma_{12}^{(1)}(\Delta t) = \rho_U(\Delta \underset{\sim}{x}_o) \exp(-j2\pi \nu_o \Delta t), \tag{22}$$

where ρ_U is the mutual correlation coefficient of the amplitude at two object points. The fading contrast, C_b, is then time-independent:

$$C_b^2 = A^{-2} \int d^2x_{i1} \int d^2x_{i2} \, |\gamma_{12}|^2 \tag{23}$$

c. Polychromatic Illumination

Case (b) can be generalized to include frequency diversity techniques, which decrease the contrast of the speckle pattern. Let the target be illuminated with M monochromatic laser lines, of equal strength but different frequencies. The illumination field is

$$V_M^{(1)} = U(\underset{\sim}{x}_o) \sum_{m=1}^{M} \exp[-j2\pi\nu_m t] \tag{24}$$

The instantaneous image field, $V_M^{(3)}$, is then a superposition of M contributions,

$$V_M^{(3)}(\underset{\sim}{x}_i, t) = \sum_{m=1}^{M} V_m^{(3)}(\underset{\sim}{x}_i, t) \, . \tag{25}$$

Upon integrating the instantaneous irradiance distribution, $I_M = |V_M^{(3)}|^2$, over a time, T, long enough to average out all beat frequency terms, the irradiance becomes a sum of irradiances, one for each laser line, and the energy deposited on the detector, W_M, is

$$W_M = T \int d^2x_i \sum_{m=1}^{M} |V_m^{(3)}(\underset{\sim}{x}_i)|^2 \tag{26}$$

Assuming that all contributions are of equal strength and stationary, the square of the contrast, C_M, is

$$C_M^2 = M^{-2} A^{-2} \int d^2x_{i1} \int d^2x_{i2} \sum_{m,n=1}^{M} |\gamma_{12,mn}|^2 \qquad (27)$$

where, by a simple extension of (18),

$$\gamma_{12,mn} = \int d^2x_{o1} \int d^2x_{o2} H_{12,mn}(\underset{\sim}{x}_{o1}, \underset{\sim}{x}_{o2}) \phi(k'_m, -k'_n) \rho_\eta(\Delta \underset{\sim}{x}_o) \gamma_{12}^{(1)}(0). \qquad (28)$$

If the laser lines are dense enough to allow replacement of the summation over lines by integration over frequency, the energy W_c becomes

$$W_c = \int d^2x_i \int d\nu \, S(\nu) \, I(\underline{x}_i, \nu), \qquad (29)$$

where $S(\nu)$ is the strength of illumination at frequency ν, attenuated by the reflection coefficient, η, which is assumed to be frequency-independent and uniform across the object. The spatial integrand is the image intensity distribution from quasimonochromatic illumination of the object, with a coherence time that does not satisfy the condition for cross-spectral purity and is much shorter than the integration time. This model for the image intensity has been used to study polychromatic speckle patterns.[18-21] Postulating, for simplicity, uniform $S(\nu)$ between ν_1 and ν_2, the square of the contrast is

$$C_c^2 = B^{-2} A^{-2} \int d^2x_{i2} \int_{\nu_1}^{\nu_2} d\nu_m \int_{\nu_1}^{\nu_2} d\nu_n \, G_{12;mn}^2 \qquad (30)$$

where $B = \nu_2 - \nu_1$ is the overall bandwidth and $G_{12,mn}$ is the Fourier transform of $\gamma_{12,mn}$[17].

2.3.2 SNR for Rough and Specular Surfaces

The main results of the previous section, Eqs. (20, 23, 27, 30), are valid when the field at the image plane is a spatially complex Gaussian process. It has been shown, experimentally by Ohtsubo and Asakura[22] and theoretically by Goodman[23], that this assumption is valid for sufficiently rough surfaces. Considerable effort has been devoted recently to a study of the effects of surface roughness on the contrast of monochromatic[8, 22, 23] and polychromatic speckle patterns[18-21]. Qualitatively, for smoother surfaces the random phase modulation of the field leaving the object is distributed over a range narrower than $\pm\pi$, the corresponding field at the image can not be treated as a complex Gaussian process, and the contrast of the speckle pattern, measured as $\sigma_I / \langle I \rangle$, is smaller than unity, decreasing as the surface roughness decreases. At the limit of specular surfaces the joint characteristic function of surface roughness approaches unity. For monochromatic and polychromatic illumination the corresponding energies deposited at the detector become deterministic and the contrasts are zero. In case (a) the contrast depends only on the temporal behavior of the field.

Surface roughness is treated here as a stationary, zero-mean Gaussian process. The joint characteristic function required for computation of γ_{12} and $\gamma_{12;mn}$ is given by

$$\phi(k_1, k_2) = \exp\left[-\frac{1}{2}\sigma_z^2 (k_1^2 + k_2^2 + 2k_1 k_2 \rho)\right], \qquad (31)$$

where $\rho(\Delta \underline{x}_o)$ is the normalized correlation of the surface profile

$$\rho(\Delta \underline{x}_o) = \langle z(\underline{x}_{o1})\, z(\underline{x}_{o2}) \rangle / \sigma_z^2 \,. \tag{32}$$

To gain more qualitative insight into the effects of surface structure on the degree of coherence of the image field, let the correlation function $\rho(\Delta \underline{x}_o)$ fall quadratically from unity near the origin, with width a; $\rho \approx 1 - |\Delta \underline{x}_o|^2/a^2$. Then the required characteristic function's dependence on $\Delta \underline{x}_o$ is, approximately,

$$\phi(k', -k') \approx \exp[-(k'\sigma_z)^2 |\Delta x_o|^2/a^2]. \tag{33}$$

Takai[24] has shown that the above approximation for a Gaussian correlation is accurate within a few percent for $k'\sigma_z \geq \pi$. Furthermore, for large $k'\sigma_z$, the function can be approximated by

$$\phi(k', -k) \approx \pi \left(\frac{a}{k'\sigma_z}\right)^2 \delta(\Delta \underline{x}_o) \tag{34}$$

and, similarly,

$$\phi(k'_m, -k'_n) = \exp[-\frac{1}{2}\sigma_z^2 (k'_m - k'_n)^2] \frac{\pi a^2}{k'_m k'_n \sigma_z^2} \delta(\Delta \underline{x}_o) \,. \tag{35}$$

Physically, these approximations imply that, for rough surfaces ($\sigma_z \geq \lambda$), the structure behaves as if it were composed of point scatterers, and the object is spatially incoherent. This model was used by Goodman[25] and many others[2-7] to study speckle pattern statistics.

Let $^*W$ and ^oW denote the energies deposited on the detector for images of rough and smooth surfaces, respectively. The corresponding contrasts for cases a, b and c will be discussed for different ratios of

coherence time and coherence area to the integration time and detector aperture. Consider first $^*W$ under condition (a) of cross spectral purity. Substituting (34) for $\phi(k',-k')$ in (19), we obtain the well-known Van Cittert-Zernike theorem[26] that the spatial degree of coherence $^*\gamma_{12}$ equals the autocorrelation function of the impulse response:

$$^*\gamma_{12}(0) = \int d^2x_o \, H_{12}(\underset{\sim}{x}_o, \underset{\sim}{x}_o), \tag{36}$$

as appropriate for an ideal diffuser. With the spatial and temporal coherence separated, the fading contrast becomes

$$^*C_a^2 = \begin{cases} 1 & \text{for } A_3 >> A, \; T_3 >> T \\ \dfrac{A_3}{A} \quad \dfrac{T_3}{T} & \text{for } A_3 << A, \; T_3 << T \end{cases} \tag{37}$$

where Mandel's definitions of coherence area A_3 and coherence time T_3 are employed:

$$A_3 = \int d^2x \, |\gamma_{12}(\underset{\sim}{x})|^2 \tag{38}$$

$$T_3 = \int dt \, |\gamma_{11}(t)|^2 \tag{39}$$

For specular surfaces, $\phi(k',-k') = 1$ and the degree of spatial coherence is given by

$$^o\gamma_{12} = \int d^2x_{o1} \int d^2x_{o2} \; H_{12}(\underset{\sim}{x}_{o1}, \underset{\sim}{x}_{o2}) \rho_\eta(\Delta \underset{\sim}{x}_o) \, \gamma_{12}^{(1)} . \tag{40}$$

For uniform illumination ($\gamma_{12}^{(1)} = 1$) and uniform reflection ($\rho_\eta = 1$), it follows that $|^o\gamma_{12}| = 1$. Then the fading contrast is given by

$$ {}^{o}C_a^2 = \begin{cases} 1 & \text{for } T_3 >> T \\ \frac{T_3}{T} & \text{for } T_3 << T \end{cases} \tag{41} $$

For specular surfaces, fading becomes minimal when the coherence time is very short with respect to the integration time, regardless of the detector aperture.

b. In the case of monochromatic illumination, the degree of coherence for a rough scatterer is only spatial and the contrast is given by

$$ {}^{*}C_b^2 = \begin{cases} 1 & A_3 >> A \\ A_3/A & \text{for } A_3 << A \end{cases} \tag{42} $$

For specular surfaces ${}^{o}W_b$ is deterministic and

$$ {}^{o}C_b = 0 \tag{43} $$

c. Lastly, we return to the case of polychromatic illumination. The general expression (27) for C_M^2 can be evaluated for rough surfaces by substituting (35) into (19) for $\gamma_{12;mn}^{(3)}$. Assuming that the wavelength dependence of the PSF is negligibly small[27], and that adjacent lines are separated in frequency by $\Delta\nu$, the contrast is expressible as

$$ {}^{*}C_M^2 = \frac{{}^{*}C_b^2}{M}\left[1+\frac{2}{M}\sum_{n=1}^{M-1}(M-n)\exp(-b^2n^2)\right] \tag{44} $$

where $b = 2\pi(\Delta\nu\,\sigma_z/c)(1+\cos\theta)$. This predicts that the contrasts for the limiting cases of complete correlation (all lines have the same frequency) and large decorrelation (large $\Delta\nu$) are equal to ${}^{*}C_b^2$ and to ${}^{*}C_b^2/M$, respectively. The result can be simplified for the following limited cases:

$$ {}^{*}C_M^2 = \begin{cases} 1 & \Delta\nu = 0 \quad \text{and} \quad A_3 >> A \\ 1/M & \Delta\nu > c/\sigma_z \quad \text{and} \quad A_3 >> A \\ (A_3/A)/M & \Delta\nu > c/\sigma_z \quad \text{and} \quad A >> A_3 \end{cases} $$

For the specular, deterministic case, ${}^{o}C_M^2 = 0$.

For polychromatic illumination of continuous spectrum, the contrast is obtained from (30), using (35), yielding

$$ {}^{*}C_c^2 = \frac{{}^{*}C_b^2}{B^2} \int_{\nu_1}^{\nu_2} d\nu_m \int_{\nu_1}^{\nu_2} d\nu_n \exp[-(k'_m - k'_n)^2 \sigma_z^2] \qquad (46) $$

or[21]

$$ {}^{*}C_c^2 = {}^{*}C_b^2 \left[\frac{\pi^{1/2}}{\beta} \operatorname{erf}\beta - \frac{1-\exp(-\beta^2)}{\beta^2} \right] \qquad (47) $$

where $\beta = 2\pi(B\sigma_z/c)(1+\cos\theta)$. The contrast decreases with increasing bandwidth B. Again, for the specular case, ${}^{o}C_c^2 = 0$.

The ratio A_3/A in the limiting expressions for the contrast reveals that it is possible to improve fading-limited SNR by spatial averaging over many coherence areas; the method will be discussed in more detail in Section 2.5. For cross-spectrally pure light the improvement in SNR can be obtained by temporal averaging over many coherence times of the illumination. For polychromatic illumination a gain in SNR can be obtained from an increase in frequency separation between the lines, or an increase in bandwidth of the illumination. As an example, consider the situation presented in Fig. 2, showing three distinct kinds of image resolution cells observable in laser-illuminated systems. Cell 1 is specular; cell 2 is optically rough but nearly normal to the line of sight;

cell 3 is also rough but lies skewed to the line-of-sight and has a considerable depth R_d, much larger than the roughness scale. Assuming the same average energy from all three resolution cells, the fading-limited SNRs evaluated for each cell are different. Cell 1 does not fade at all in coherent illumination, but image cells 2 and 3 will fade considerably. The cells will also behave differently as the coherence time of the illumination is shortened, or, equivalently, as the bandwidth is broadened. Cell 1 will still be free of fading; the fading of cell 2 will diminish slightly; the fading of the "deep" resolution cell 3, will diminish most rapidly because the controlling dimension of this cell is not the roughness but the depth of the cell.

Figure 3 presents fading-limited SNRs for discrete frequencies (solid line) and for a continuous spectrum (dashed lines) vs. the total illumination bandwidth, for different scales of roughness. For discrete multiline illumination, the smallest and largest frequency differences between lines are $\Delta\nu = B/(M-1)$ and B respectively. The SNR ranges from 1 to $M^{1/2}$, the latter being obtained when the sum in (44) is negligible compared to unity. For the case of two lines, and to reduce this sum to less than 0.01, the bandwidth $B=\Delta\nu$ must exceed $2.14(c/4\pi\sigma_z)$. Thus, to decorrelate two speckle patterns, each due to a single line illuminating a surface with $\sigma_z = 1\,\mu m$, the frequency offset cannot be smaller than 50 THz. For wider bandwidths, the SNR is greater when more lines are used, but for smaller bandwidths, the SNR is seen to be larger for M=2 than for M=11. This can be explained by

examination of the sum in (44), which has M-1=10 terms, only one of them smaller than 0.01. There are 10 terms offset in frequency by B/10, 9 terms by B/9, 8 terms by B/8, etc. It follows that if the total bandwidth is ten times broader than the minimum $\Delta\nu$, a surface roughness with $\sigma_z = 1\mu m$ mutually decorrelates all eleven speckle patterns and the corresponding SNR is equal to $\sqrt{11}$. Generally, for a fixed total bandwidth B and surface roughness σ_z, the SNR is larger for a smaller number of lines than for more lines when the bandwidth is less than the one that decorrelates the speckle patterns corresponding to the smaller number of lines.

For a given degree of roughness, the SNR for a larger number of lines is well approximated by that for a continuous spectrum when the bandwidth is smaller than $(M-1)c/2\pi\sigma_z$, for which not all the speckle patterns are decorrelated. For wider bandwidths, the SNR can be well approximated by $M^{1/2}$ and $(\beta^2/\pi)^{1/4}$ for discrete and continuous spectra, respectively. The significant difference between the two wideband cases is that the discrete-spectrum SNR is independent of bandwidth, while the continuous-spectrum SNR is proportional to the square root of the bandwidth.

Typical material roughness may vary from fractions of a micrometer to several tens of micrometers. For a surface with $\sigma_z = 1\mu m$ illuminated with radiation covering the visible region 0.4 μm-0.7 μm (B=321 THz) the SNR ≈ 3. An Ar laser generating 4 lines at .514, .494, .484, and .474 μm, was used in the first experiment

testing the usefulness of the frequency diversity technique for decreasing the speckle contrast[6]. The experiment has shown that the contrast of a superposition of speckle patterns, each due to a single line diffracted by a rough surface with $\sigma_z > 10\ \mu m$ and each with unity contrast, is noticeably smaller then unity. Fig. 3 confirms that, even for the smallest frequency offset between the lines, $B = 12.6$ THz, there is some decorrelation.

2.4 SNR for Low-Level Signal

Consider first the case when there is no fading ($C_W = 0$) and the SNR reduces to $\langle n_S \rangle / [\langle n_S \rangle + \langle n_N \rangle]^{1/2}$. By the preceding discussion, this formula is valid when temporally coherent and partially coherent illumination fields are reflected from specular surfaces. Fading limits the SNR only for strong signals, since it adds $C_W^2 \langle n_S \rangle^2$ to the noise term above; see (8). Figure 4 is a typical plot of SNR as a function of signal $\langle n_S \rangle$ for particular levels of noise $\langle n_N \rangle$ and fading contrast C_W. For spectrally pure and for monochromatic illumination, C^2_W is the inverse of the number of degrees of freedom in the field across the detector. This number becomes the effective number of spatial modes, A/A_3, or the number of temporal modes, T/T_3, whenever either of these is large, or the number of spatio-temporal modes, $(A/A_3)(T/T_3)$, when both are large. With no background light or fading, the SNR is signal-shot-noise limited and equal to the square root of the number of signal photo-electrons; this is the middle asymptote in the figure. The background

noise-limited asymptote, for weak signals, is proportional to $\langle n_S \rangle$. The asymptotic fading-limited SNR, for strong signals, is independent of $\langle n_S \rangle$ and equal to the inverse of the fading contrast. The graph shows the combined effects of signal photocounts, background and dark current counts, and fading due to partial coherence in determining the detector SNR.

2.5 Trade-Off of Spatial Resolution and SNR

To maximize the spatial resolution of the stationary imaging system, the detector aperture is normally made no larger than the diffraction-limited resolution cell of the telescope. In many situations, it may be desirable to improve the SNR at the expense of resolution. Larger apertures can increase the SNR by reducing fading contrast. The nature of this trade-off may be appreciated by considering a uniformly illuminated and uniformly reflecting target viewed against a uniform background and taking as the reference SNR the one associated with the output of a detector having an aperture that matches the diffraction-limited resolution cell of the telescope.

In the general expression (8) for SNR, both $\langle n_s \rangle$ and $\langle n_N \rangle$, the expected numbers of signal and noise counts, are proportional to the area A of the detector aperture. On the other hand, C_W^2 is inversely proportional to A, whenever it can be approximated by A_3/A. Dainty[28] has shown that this is valid when A/A_3 exceeds 5 and that C_W^2 is only slightly larger than A_3/A when $1 < A/A_3 < 5$. Furthermore, for spatially

incoherent, well-resolved objects, the diffraction-limited resolution cell[3, 4] and the coherence area at the image plane, A_3, are the same size. It follows that both $C_W^2 \langle n_s \rangle$ and $\langle n_N \rangle / \langle n_s \rangle$ are approximately independent of the detector area, so that the SNR in (8) varies as $A^{1/2}$. One concludes that an improvement in SNR can be traded against a loss of resolution proportional to the square of the enhancement in SNR, or else in direct proportion to it when only linear resolution is considered.

2.6 Conclusions

For images of actively illuminated targets detected by a photon counting array, the SNR is affected by the coherence of the radiation, the roughness of the target and the PSF of the optical system, as well as by the aperture and integration time of the detector. All these effects can be accounted for in a compact expression, (8), for the SNR, by introducing the fading of the signal across the detector and the fading contrast C_W, which generalizes the speckle contrast. The expression indicates that, for increasing signal levels, the SNR is limited first by background noise, then by signal shot noise, and ultimately by the fading.

The fading contrast involves stochastic, spatial, and temporal averaging of the second moment of the irradiance, or the degree of coherence, which propagates from the rough target to the image plane. The roughness enters by way of the joint characteristic function of the surface statistics. For a resolution cell skewed with respect to the direction of observation, it is the depth of that cell that plays the role

of the roughness scale.

The expressions obtained for the fading contrast reveal quantitatively the efficiency of various means for improving fading-limited SNR, by temporal averaging, by spatial averaging, or by increased bandwidth of illumination. Plots of the SNR against bandwidth for various roughness scales and against signal strength for various noise and fading levels have been presented and it has been shown that the SNR can be improved at the expense of spatial resolution.

2.7 References

1. H.H. Hopkins, Proc. Roy. Soc., A208, 408 (1953).

2. Y. Ichioka, J. Opt. Soc. Am., 64, 919 (1974).

3. L.H. Enloe, BSTJ, 46, 1479, (1967).

4. S. Lowenthal and H.H. Arsenault, J. Opt. Soc. Am., 60, 1478 (1970)

5. J.D. Dainty, Optica Acta, 18, 327 (1971).

6. M. Elbaum, M. Greenebaum, and M. King, Opt. Commun. 5, 171 (1972).

7. M. George and A. Jain, Appl. Physics, 4, 201 (1974).

8. H. Fujii and T. Asakura, Opt. Commun., 11, 351, (1974).

9. J.W. Goodman, Proc. IEEE, 53, 1688 (1965).

10. E. Wolf, Proc. Ray. Soc. (London) A230, 246 (1955).

11. L. Mandel, Proc. Phys. Soc., (London) 74, 233 (1959).

12. J. Bures, J. Opt. Soc. Am., 64, 1598, (1974).

13. K.W. Pratt, "Laser Communication Systems," (Wiley, New York, 1969).

14. The contrast of speckle patterns formed with partially coherent light at the image plane of a diffusing object has been studied by Fujii in Asakura (Opt. Commun. 12, 32, (1972), and Nouv. Rev. Optique, 6, 5, (1975).

15. K. Miller, SIAM Rev., Vol. 11, (Oct. 1969).

16. The assumption that the field is a complex Gaussian stochastic process is not necessary to validate (11). It has been shown by Chen and Tartaglia (Opt. Commun. 6, 119 (1972)) that when laser light is scattered from an assembly of N independent particles,

$$\langle I(x_1)I(x_2)\rangle = \langle I\rangle^2 + (1+N^{-1})\,|\Gamma(x_1-x_2)|^2 .$$

N is a large in our case.

17. L. Mandel, J. Opt. Soc. Am., 51, 1342, (1961).

18. J. Fujii and T. Asakura, Optik 39, 284, (1974).

19. G. Parry, Optica Acta, 21, 763, (1974).

20. H. M. Pedersen, Optica Acta, 22, 523, (1975).

21. H. M. Pedersen and C. T. Stansberg Opt. Commun., 15, 222, (1975).

22. J. Ohtsubo and T. Asakura, Opt. Commun., 14, 30, (1975).

23. J. W. Goodman, Opt. Commun., 14, 324, (1975).

24. N. Takai, Japanese J. of Applied Phys., 13, 2025, (1974).

25. J. W. Goodman, Stanford Electronics Laboratory Report, Stanford, California (1963).

26. J. Perina, "Coherence of Light," (Van Nostrand Reinhold Company, Ltd., 1972).

27. The dependence of speckle contrast computed without this assumption has been studied in (7) and (19).

28. J. C. Dainty, Optica Acta, 17, 761 (1970).

2.8 Figure Captions

Fig. 1 Geometry of the imaging system. 0 = object, T = imaging lens, I = image, A = array of detectors.

Fig. 2 Imaging of rough target, showing various object resolution cells: 1 = specular, 2 = optically rough but nearly normal to the line-of-sight, 3 = optically rough but skewed to the line-of-sight.

Fig. 3 Fading-limited SNR for discrete frequencies (solid lines) and for a continuous spectrum (dashed lines) vs. the total illumination bandwidth, for different scales of roughness, assumed greater than the illumination wavelength.

Fig. 4 Typical plot of SNR vs. signal level, $\langle n_s \rangle$, with its asymptotic approximations. The steepest asymptote is for background-noise-limited operation: SNR = $\langle n_s \rangle / \langle n_N \rangle^{1/2}$. The middle asymptote is for signal-shot-noise-limited operation: SNR = $\langle n_s \rangle^{1/2}$. The horizontal asymptote represents target-fading limitation: SNR = C_w^{-1}. Noise level $\langle n_N \rangle = 9$, fading contrast $C_w = 0.1$.

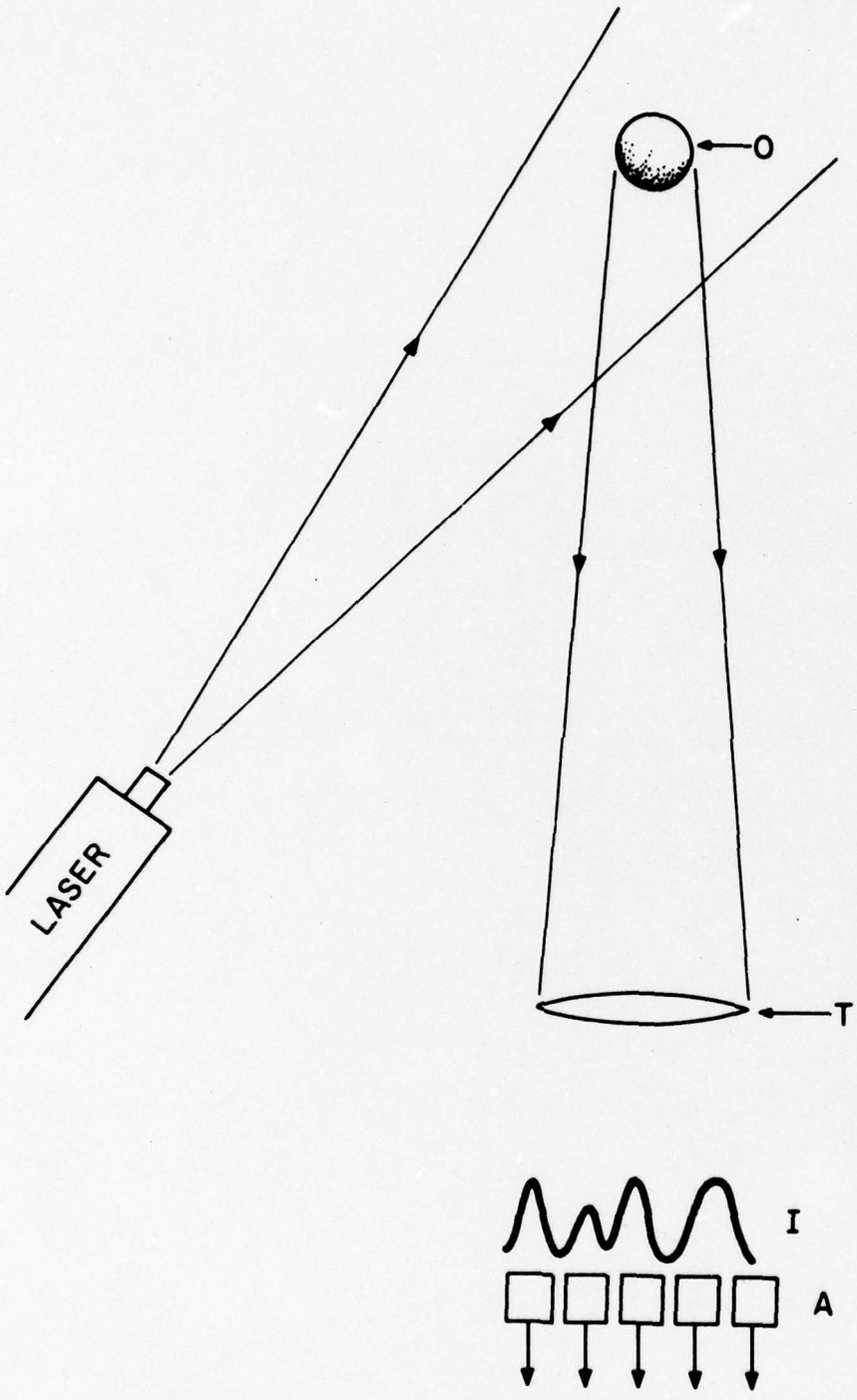

Fig. 1

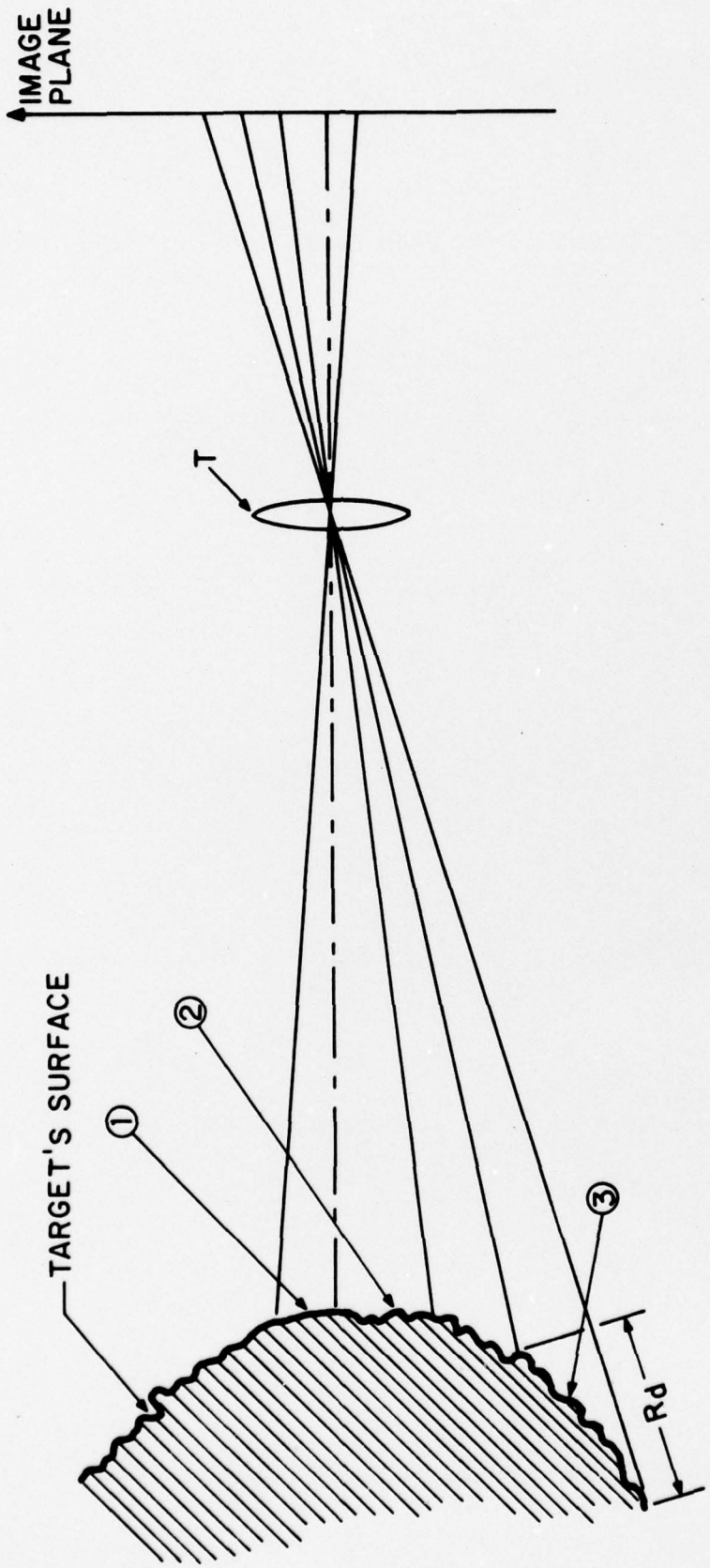

Fig. 2

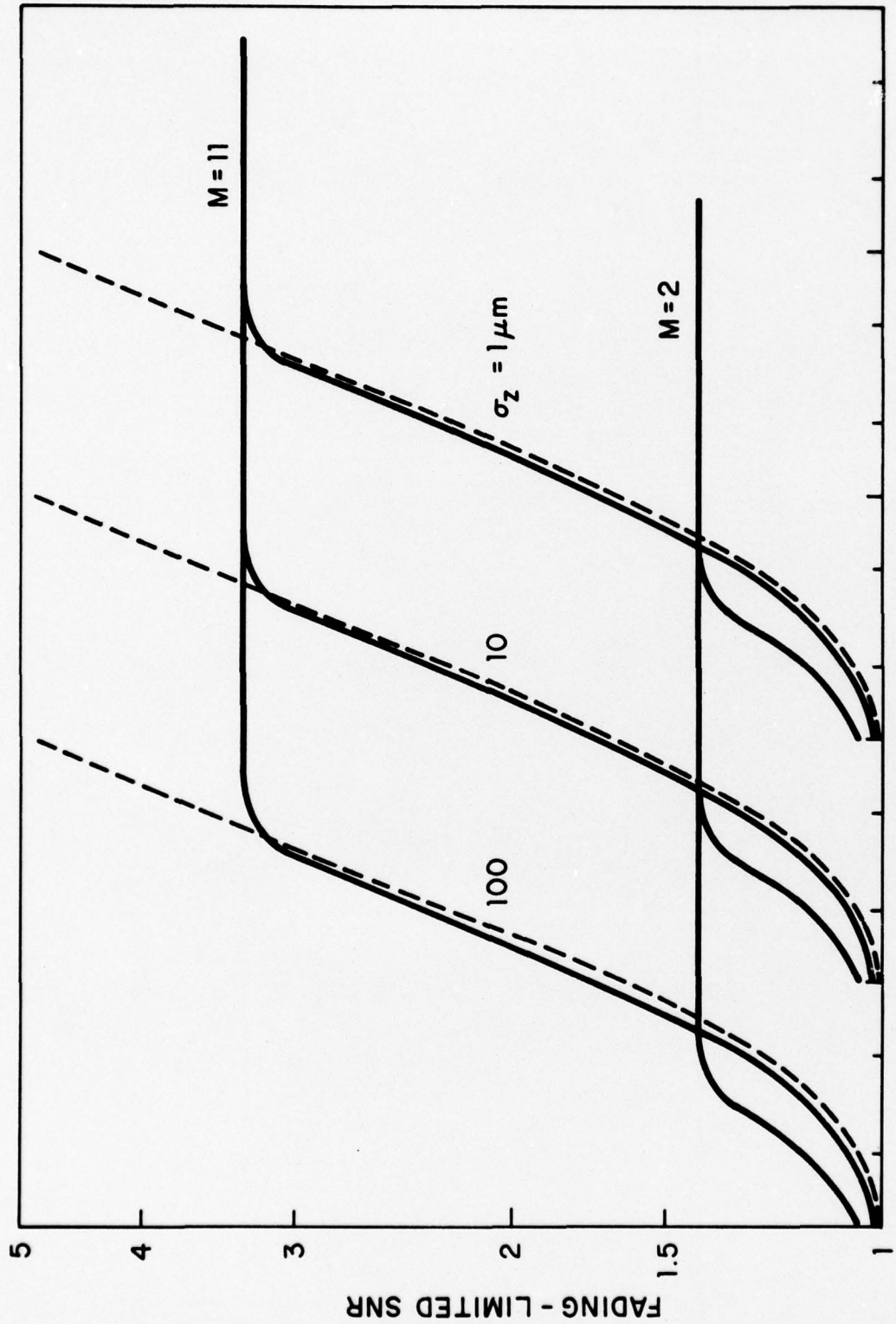
FADING - LIMITED SNR
5
4
3
2
1.5
1
0.1
1
10
100
1000
ILLUMINATION BANDWIDTH (THz)
M=11
M=2
σ_z = 1 μm
10
100

Fig. 3

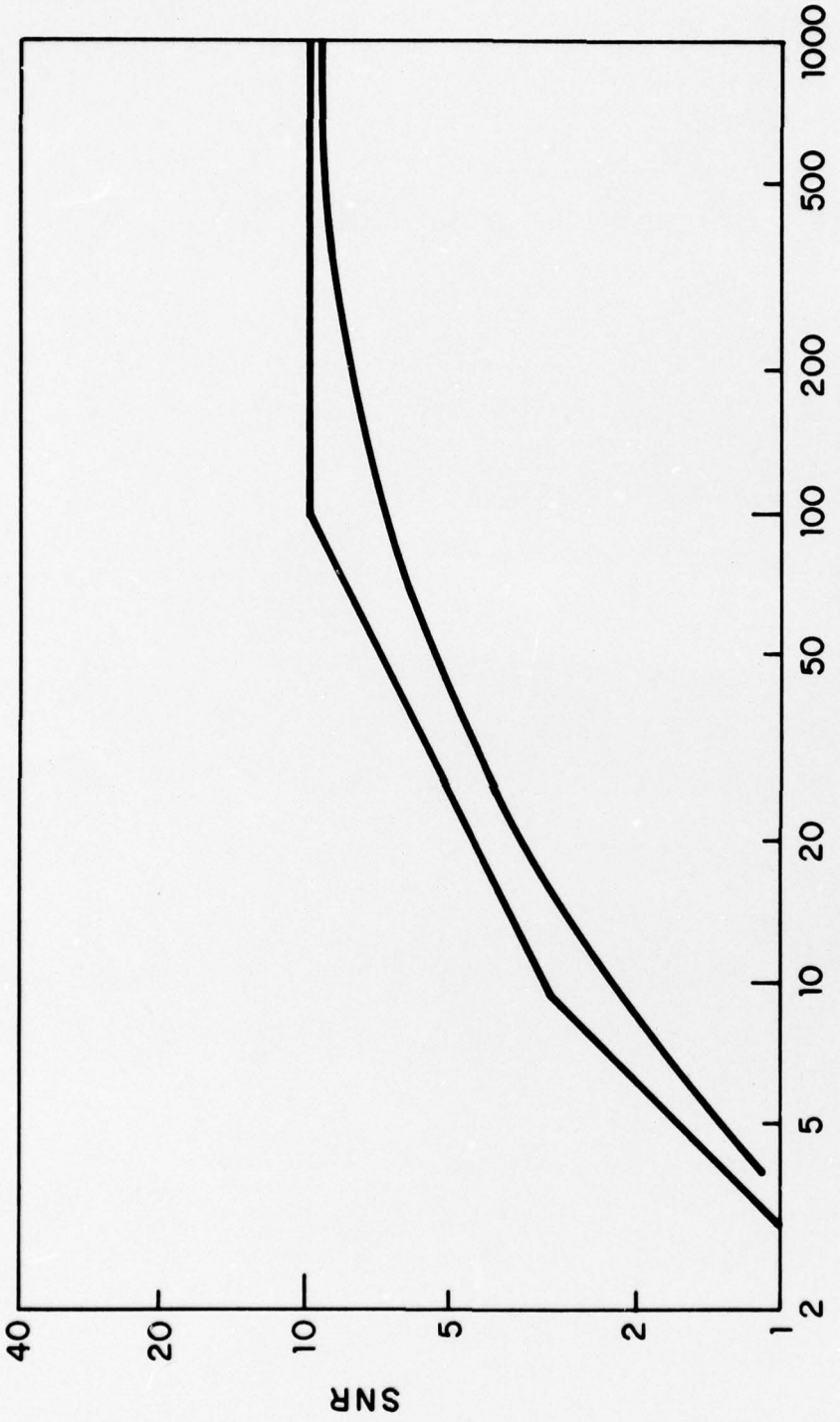
SNR
40
20
10
5
2
1
2
5
10
20
50
100
200
500
1000
NUMBER OF SIGNAL PHOTOELECTRONS

Fig. 4

III. MAXIMUM ANGULAR ACCURACY OF PULSED LASER RADAR IN PHOTOCOUNTING LIMIT

To estimate the angular position of targets with pulsed laser radars, their images may be sensed with a four-quadrant noncoherent detector and the image photocounting distribution processed to obtain the angular estimates. The choice of estimator depends on the statistics of the photocounts, which reflect those of the energy deposited on the detectors by the laser field returned from the target. For an optically rough target, this is a spatio-temporal complex Gaussian process, producing photoelectrons that obey a negative binomial distribution with M degrees of freedom. The limits imposed on the accuracy of angular estimation by signal and background radiation shot noise, dark current noise and target cross-section fluctuations are calculated. Maximum likelihood estimates of angular positions are derived for optically rough and specular targets and their performances compared with theoretical lower bounds. These estimates are realizable in systems with automatic gain control, fast enough to follow the random fluctuations of the target returns. For slower systems and large signals, the accuracy of the resulting estimates is limited by target fluctuations.

Portions of these results were presented at the 1975 meeting of the Opt. Soc. of Am. in Boston, J. Opt. Soc. Am., 65, 1204A, with M. King, W. Edelson and P. Diament.

Accepted for publication in Appl. Optics, with P. Diament, M. King and W. Edelson.

3.1 Introduction

The potential of considerably higher accuracy than that of microwave radars motivates interest in employing laser radar for angle tracking. With the advent of high-power lasers, angle-tracking laser radars are particularly attractive for spaceborne applications because the absence of atmospheric turbulence allows their potential for high accuracy to be used to full advantage. In certain satellite tracking applications, objects at distances of megameters must be positioned to decimeters. High-accuracy tracking, used for precisely pointing a communication laser beam from one satellite to another, promotes efficient use of laser energy in the communication link. It has also been pointed out[1] that precise knowledge of the relative positions of two spacecraft performing a rendezvous maneuver is often impractical to obtain from ground-based radars; an accurate laser radar located on board the spacecraft could serve as a guidance aid.

In an angle-tracking system, a sequence of direct measurements of target position is fed into a tracking filter which may produce refined estimates of past, present, and future target position. Generally, the accuracy of the refined estimate is proportional to the accuracy of direct measurements, so that

schemes for improving measurement accuracy are potentially of great significance.

Maximum likelihood estimation of the location of an optical object has been studied by Saleh,[2] who considered shot-noise-limited detection of the images. McGarty[3] has investigated estimation of the optical position of the centroid of the image photocounting distribution (IPD). The properties of the IPD have been analyzed by Amoss and Davidson[4] in the context of detection of weak optical images, and by Helstrom,[5,6] who considered object radiation in the presence of uniform background noise. All these papers have considered only self-illuminated noncoherent objects.

This paper considers the estimation of angular positions of laser-illuminated optically rough and specular targets from their images. The field of the returned laser light is treated as a spatio-temporal stochastic process that forms the image irradiance distribution (IID), which is sensed by a four-quadrant detector and converted into the IPD. An estimate of the target angular position (TAP) is obtained by splitting and differencing the IPD.

The accuracy of estimates of optical-image TAP based on four-quadrant detection has been evaluated in the past by adapting conventional microwave radar theory.[7-9] The optical analogue of the classical microwave beam-slitting formula,

$$\sigma = g\ (\lambda/D)/\mathrm{SNR}\ , \qquad (1.1)$$

indicates that the RMS error σ is proportional to the optical system resolution (λ/D) and inversely proportional to the detected SNR, through some function g of the image distribution.

However, three important differences suggest that the accuracy of TAP estimates for laser radar systems may not be the same as for microwave radar systems. First, the laser system can employ noncoherent (or direct) detection of the target return to extract the angular position. Second, the quantum noise may be quite apparent in the laser system, though insignificant in the microwave system. Finally, the laser system can resolve targets with modest-size telescope apertures while the microwave system deals primarily with unresolved objects.

This paper considers targets considerably smaller than a diffraction-limited resolution cell of the imaging telescope. The case of a target that extends over many such resolution cells has also been considered[10] and will be discussed in a forthcoming paper. The TAP is estimated directly from the outputs of the photodetectors, which sense a single-look IID. During this single look, the target does not translate with respect to the optical line-of-sight; target rotation is permitted during a look, however, so long as the noncoherent reflectance distribution of the target remains unchanged, within the resolution limit of the imaging telescope. The mean and standard deviation of the single-look TAP estimates are derived,

and the limitations imposed by laser speckles, photocounting, background, and dark current noise on the accuracy of the estimates are investigated.

3.1.1 Mathematical Idealizations

In order to concentrate on essential considerations, several assumptions have been made in this analysis. First, let the uniformly reflective, optically rough target be illuminated by a linearly polarized laser beam of wavelength λ. The rough-surface height profile is regarded as a spatially stationary random process with standard deviation σ_s and coherence area ρ_s and does not alter the polarization of the incident light. The target size is taken to be smaller than the coherence volume associated with the laser illumination.

The aberration-free imaging system has a loss-free square pupil of side D, an effective focal length F, a space-invariant coherent point spread function (PSF) h, and is situated in the far field of the target at a distance R from it. The areas of the diffraction-limited resolution cells at the target and image planes are, respectively, $A_0 = (\lambda R/D)^2$ and $A_i = (\lambda F/D)^2$. The area A_0 is assumed to be much larger than the target, whose surface contains many surface-coherence areas, ρ_s.

The detectors are assumed to be ideal photon-counting devices with an ideal time response, identical quantum efficiencies η, and uniform spatial responsivity.

3.1.2 Noise Source

The sources of noise considered in this analysis are target fading, signal and background light shot noise, and dark current. These are discussed briefly in the following paragraphs.

According to the scalar theory of diffraction, the spatial coherence of the illumination is destroyed by surface roughness when $\sigma_s \gg \lambda$.[11,12] In that case, the field returned from the target can be treated as a superposition of temporally coherent fields originating at spatially independent scatterers on the target surface, with each one introducing into the outgoing wave a random, uniformly distributed phase shift. Since the total number of scatterers is large (approximately equal to the ratio of the illuminated target area to the surface coherence area ρ_s[13]), the central limit theorem implies that the field returned from the target is a stationary, zero-mean, complex Gaussian process over the receiver aperture plane.[11] In general, the coherence area of this field can be obtained from the Van Cittert-Zernike theorem.[14] For instance, if the target is a sphere of radius r, then the coherence area is given by $A_2 \approx \pi \cdot (0.6\ \lambda R/2r)^2$. It follows that, under the assumptions made, the receiver aperture is smaller than A_2.

When the target rotates, the receiver pupil plane field becomes a spatio-temporal complex Gaussian process[17] with coherence time T_2 equal to the time it takes for the coherence area A_2 to travel across a point aperture. Therefore the coherence times of the pupil plane field and of the corresponding image field are equal.

It follows that the instantaneous image irradiance distribution $I(\underline{x}_i,t)$ is a spatio-temporal process, obeying a negative exponential probability density function (PDF) with parameter $\langle I(\underline{x}_i,t)\rangle$, the mean irradiance.

The energy deposited on a detector of area A during time T is:

$$W = \int_A d^2\underline{x}_i \int_T dt\, I(\underline{x}_i,t) \quad . \tag{1.2}$$

In this analysis we refer to the fluctuations in W as the target-fading noise. The deposited energy W is assumed to obey a gamma PDF with parameter γ and M degrees of freedom. If T_3 is the coherence time of the image-plane field and A_3 is its area, the number of degrees of freedom is:

$$M = (T/T_3)(A/A_3) \quad \text{for} \quad T \gg T_3 \quad \text{and} \quad A \gg A_3 \tag{1.2a}$$

$$M = A/A_3 \quad \text{for} \quad T \ll T_3 \quad \text{and} \quad A \gg A_3 \tag{1.2b}$$

$$M = T/T_3 \quad \text{for} \quad T \gg T_3 \quad \text{and} \quad A \ll A_3 \tag{1.2c}$$

$$M = 1 \quad \text{for} \quad T \ll T_3 \quad \text{and} \quad A \ll A_3 \tag{1.2d}$$

Mandel has shown[19] that Eq. (1.2a) applies well for partially coherent Gaussian light that satisfies the conditions for cross-spectral purity. Equation (1.2c) is satisfied by the noncoherent background light. Equation (1.2d) is well satisfied by monochromatic, linearly polarized laser speckle patterns,[12,13,20] and Eq. (1.2b) is a good approximation for spatially integrated laser speckle patterns.[12,13,20]

Consider also the return from a target illuminated with a multiline laser. For optically rough targets, all components of the fields are stationary complex Gaussian processes over space. The components, taken to be of equal strength for simplicity, can be treated as statistically independent if the frequency offsets between the lines are sufficiently large to allow the rough surface to produce spatially decorrelated speckle patterns.[12,22,23] For an integration time long enough to average out the beat frequency cross terms, the resulting energy obeys a gamma PDF with the number of degrees of freedom equal to the number of laser lines.

In this analysis we will often use as the fading-limited SNR the ratio of the mean to the standard deviation of W. It can be shown that in many situations of interest, this ratio is equal to the inverse of the square root of the number of degrees of freedom.[12,13,18]

Spatially incoherent background noise with a coherence time much shorter than the integration time T is assumed.

Photocounting noise results from the random fluctuations of the total number of photocounts, m, at the detector's output. The number m is a sum of three terms: the counts generated by the noisy signal W, the counts due to the background radiation, and the dark current counts. The three terms are mutually independent; the first one is a doubly stochastic pocess,[18] the other two obey Poisson PDFs. The impact of the first term on the system performance is of particular interest here.

This analysis does not take into account the target-angle noise that may result from random fluctuations due to finite size. This effect is caused by variations in the phase front of radiation from a multiple-point target as the target changes its aspect. It has been found that in microwave monopulse the effects of this noise decrease with the target range.[26,27] Thus the angle noise can be disregarded for ranges long enough for phase-front distortions to be negligible. It is also assumed that detector and preamplifier noise have been reduced to the point where $kT \ll h\nu$, so that the Johnson noise is negligibly small. Also, 1/f noise is not considered.

3.2 Problem Formulation

The problem of TAP estimation is addressed systematically by (1) finding the theoretical limits given by the Cramér-Rao lower bounds for the standard deviations of the estimates and (2) by proposing operations on the data that lead to estimates with standard deviations that approach the theoretical lower bounds. In this paper, the Maximum Likelihood Estimates (MLE) of the TAP are considered as the candidates likely to possess the desired properties. In order to derive the Cramér-Rao bounds and the MLEs, knowledge of the joint probability density function (PDF) of the stochastic processes is required. In this section, the PDFs for the cases treated in the paper are introduced. They are used in Parts 3.3 and 3.4 for the derivations of the Cramér-Rao bounds and of the MLEs.

For the unresolved target, the image shape matches the noncoherent PSF of the imaging system and the location of the peak of the IID depends on the target location. Its peak value, and therefore the total energy in the image field, can be treated as a random variable that depends on the realizations of the field in front of the receiver aperture.

The analysis considers targets that are displaced by an unknown angle in the x direction with respect to the optical axis of the imaging system; see Fig. 1. For simplicity, only one of the two angular coordinates is treated since, for a

square aperture, the two are independent. Also, for unresolved targets the fluctuations do not depend on the segmentation. The image irradiance is redistributed between the two photodetectors by the reflective prism, the proportions depending on the TAP. If the irradiance is a temporally stationary stochastic process, the energies deposited on the two detectors during an integration time T are

$$W_1 = S_1 W \quad , \quad W_2 = S_2 W \tag{2.1}$$

where is the energy captured by the pupil aperture during time T. The fractions S_1 and S_2 depend on the noncoherent PSF, i.e., the squared magnitude of the coherent $h(x_0, y_0; x_i, y_i)$, and are given by

$$S_1 = \int_{-\infty}^{0} dx_i \int_{-\infty}^{\infty} dy_i \left| h(\theta_0 R, 0; x_i, y_i) \right|^2$$

$$S_2 = \int_{0}^{\infty} dx_i \int_{-\infty}^{\infty} dy_i \left| h(\theta_0 R, 0; x_i, y_i) \right|^2 \tag{2.2}$$

It is assumed that the PSF is normalized to fix the total energy in the intensity PSF at unity:

$$S_1 + S_2 = 1 \quad . \tag{2.3a}$$

In addition, if θ_0 is smaller than the diffraction-limited resolution of the aperture, then approximately,

$$S_1 - S_2 \approx \ell \theta_0 \quad , \tag{2.3b}$$

where ℓ is a known proportionality coefficient depending on the PSF. For the square aperture under consideration, $\ell = 2D/\lambda$.

Let the number of photoelectrons resulting from the photons arriving at the two detectors in random quantities $\eta WS_1/h\nu = NS_1$ and $\eta WS_2/h\nu = NS_2$, be n_1 and n_2, where η is the quantum efficiency of the detector, and $h\nu$ is the energy of a single photon. $N = \eta W/h\nu$ obeys the gamma PDF with M degrees of freedom[20,28] and parameter $\gamma = (M/N_s)$:

$$p(N) = \gamma^M \frac{N^{M-1}}{(M-1)!} \exp(-\gamma N) \qquad (2.4)$$

with $N \geqslant 0$ only. The limiting forms are:

$$p(N) = \exp(-N/N_s)/N_s, \quad M = 1 \qquad (2.4a)$$

$$p(N) = \delta(N - N_s) \quad , \quad M \to \infty \qquad (2.4b)$$

where $N_s = \eta \langle W \rangle / h\nu$ is the mean signal photocount collected by the pupil. Generally, as the number of degrees of freedom M grows large, the relative fluctuations in W become small; limiting forms for evaluating M were discussed in Sec. 3.1.2.

For the analysis that follows, it is useful to obtain a formula for the joint PDF of n_1 and n_2 by using the Mandel transformation[18] of the random light distribution:

$$p(n_1, n_2) = \int_0^\infty dN\, p(N) p(n_1, n_2 | N) \quad , \qquad (2.5)$$

where $p(n_1, n_2 | N)$ is the joint conditional PDF of n_1 and n_2, given the probable total number of counts, N:

$$p(n_1, n_2 | N) = \prod_{k=1}^{2} \frac{e^{-S_k N}}{n_k!} (S_k N)^{n_k} \qquad (2.6)$$

The form of the Mandel transformation given in (2.5) uses a common value of N, rather than N_1, N_2, because in the model for unresolved targets the energies deposited on the two detectors are derived on the average from the same coherence area of the pupil plane field.

If the laser radiation returned from the target is accompanied by background noise radiation, the photocounts at the detector outputs are the sums of the signal and background counts. It is assumed that the background photocounts at each detector obey a Poisson PDF with a mean count $N_b/2$. The detector dark current noise can also contribute to the total number of counts at the detector output. It is assumed that the dark current counts of each detector obey a Poisson PDF[21] with an average count $N_d/2$. Thus, the total counts in each detector, m_1, m_2, are the sum of the mutually independent signal, background, and dark current counts. The noisy-case joint PDF of m_1 and m_2 is

$$q(m_1, m_2) = \int_0^\infty dN \; p(N) q(m_1, m_2 | N) \quad , \qquad (2.7)$$

where $q(m_1, m_2 | N)$ is the joint conditional PDF of m_1 and m_2,

$$q(m_1, m_2|N) = \prod_{k=1}^{2} \frac{e^{-(S_k N + N_N/2)}}{m_k!} (S_k N + N_N/2)^{m_k} \quad , \qquad (2.8)$$

where $N_N = (N_b + N_d)$. Equation (2.7) can be obtained directly from (2.5), for the sum of mutually independent Poisson random variables is a Poisson random variable with mean value equal to the sum of the means.[24]

The formula (2.7) can be made more suitable for deriving the MLE of the TAP if it is approximated by the expression valid for small background and dark current noises ($N_N < 1$) and for large signal-to-noise ratio ($N_S/N_N \gg 1$). Using in this formula the approximations

$$(S_k N + N_N/2)^{m_k} \cong (S_k N)^{m_k} [1 + (m_k/S_k)(N_N/2N)]$$

and

$$\exp(-N_N) \cong 1 - N_N \quad ,$$

the latter serving merely to maintain the proper normalization, the approximate joint PDF can be written as:

$$q_1(m_1, m_2) = \langle N^{m_1 + m_2} e^{-N} \rangle \frac{S_1^{m_1}}{m_1!} \frac{S_2^{m_2}}{m_2!} \left(1 - N_N + \tfrac{1}{2}\left[\frac{m_1}{S_1} + \frac{m_2}{S_2}\right]\frac{N_N}{N_M}\right) , \qquad (2.9)$$

where

$$N_M = \frac{\langle N^{m_1 + m_2} e^{-N} \rangle}{\langle N^{m_1 + m_2 - 1} e^{-N} \rangle} = \left(\frac{M - 1 + m_1 + m_2}{M + N_S}\right) N_S \quad , \qquad (2.10)$$

and the expectations are taken with respect to N, using (2.4).

For the special case when the random fluctuations of N are negligibly small (number of degrees of freedom M is large), the PDF of N can be well approximated by the Dirac delta function[28] in (2.4b). After letting the number of photocounts for this case be m_{01} and m_{02}, the joint PDF can be obtained from (2.7) and (2.8) as

$$q_0(m_{01},m_{02}) = q(m_{01},m_{02}|N_S) \quad . \tag{2.11}$$

Note that the above joint PDFs are functions of the TAP, θ_0, via the parameters S_1 and S_2.

The first problem, considered in the next section, can be stated as: given the measurements n_1 and n_2 (for a fluctuating target in the absence of background and dark current noise) and the <u>a priori</u> knowledge of N_S; or, given the measurements m_{01} and m_{02} (nonfluctuating target in the presence of background noise) and the <u>a priori</u> knowledge of N_S and N_N, what are the corresponding theoretical lower bounds for the standard deviations of the TAP estimates?

The second problem, addressed in Part 3.4, can be stated as: given n_1, n_2 and N_S, or given m_1,m_2 (fluctuating target in the presence of background noise) and N_S, N_N, and M; or given m_{01}, m_{02} and N_S and N_N, (1) find the expressions for the parameter θ_0 that maximize the joint PDFs

$p(n_1,n_2)$, $q(m_1,m_2)$, or $q_0(m_{01},m_{02})$, respectively; (2) calculate the means and the standard deviations of these expressions. It is assumed that the parameters N_S, N_N, and M are known as a result of averaging many previous measurements, or otherwise.

3.3 Lower Bounds of TAP Estimate Errors

The Cramér-Rao bound for the standard deviation of a parameter estimate provides a useful reference for the evaluation and comparison of the operations that can be performed on the data to estimate the parameter. A theorem cited by Cramér[15] states that the variance of a regular and unbiased estimate can never fall below a certain limit, dependent only on the joint PDF of the data and the size of the data sample. Specifically, if $P(\theta)$ and θ^* are the PDF of the data and a regular unbiased estimate of θ then, for a single measurement the variance of θ^* satisfies the inequality:

$$\text{var } \theta^* \geq \langle [\partial \ln P/\partial\theta]^2 \rangle^{-1} \qquad (3.1)$$

The Cramér-Rao bounds are calculated for two instructive cases of fluctuating and nonfluctuating targets in order to gain a qualitative insight into the problem of TAP estimation.

3.3.1 FLUCTUATING TARGETS, NOISELESS

For this case, the inequality (3.1) can be rewritten as:

$$\text{var } \theta_0^* \geq \langle [\partial \ln p(n_1,n_2)/\partial\theta_0]^2 \rangle^{-1} \quad , \qquad (3.2)$$

where $p(n_1,n_2)$, given by (2.5) and (2.6), depends on θ_0 only through $S_1^{n_1} S_2^{n_2}$. It follows that

$$\left\langle \left\{ \frac{\partial \ln p(n_1, n_2)}{\partial \theta_0} \right\}^2 \right\rangle = (\ell^2/4) \left\langle \left(\frac{n_1}{S_1} - \frac{n_2}{S_2} \right)^2 \right\rangle \quad . \tag{3.3}$$

The expected values $\langle n_k^2 \rangle$ $(k = 1,2)$ and $\langle n_1 n_2 \rangle$ are given by

$$\langle n_k^2 \rangle = (N_S S_k)^2 (1 + \tfrac{1}{M}) + S_k N_S \quad ; \tag{3.4}$$

$$\langle n_1 n_2 \rangle = S_1 S_2 N_S^2 (1 + \tfrac{1}{M}) \quad . \tag{3.5}$$

The inequality for the lower bound is therefore

$$\text{var } \theta_0^* \geqslant (\ell^{-2} - \theta_0^2)/N_S \quad . \tag{3.6}$$

Since θ_0 has been assumed to be much smaller than $1/\ell$, the lower bound for the standard deviation of the estimate becomes effectively

$$\sigma_{min} = 1/\ell N_s^{1/2} \quad . \tag{3.7}$$

The expression for the lower bound of the standard deviation of θ_0^* is the same as the beam splitting formula given by (1.1), with the SNR equal the square root of the signal count N_S and ℓ^{-1} proportional to λ/D. This implies that the theoretical limit for the accuracy of the TAP derived from n_1 and n_2, given N_S, is limited by signal shot noise and does not depend on target fading.

3.3.2 Nonfluctuating Targets with Noise

For nonfluctuating targets the inequality (3.1) can be rewritten as:

$$\text{var } \phi_0^* \geqslant \langle\, [\partial \ln q_0(m_{01}, m_{02})/\partial\theta_0]^2 \,\rangle^{-1} \quad , \tag{3.8}$$

where ϕ_0^* is an estimate of θ_0 and $q_0(m_{01}, m_{02})$ is given by (2.11) and (2.8).

Following the same steps as above, one has

$$\left\langle \left(\frac{\partial \ln q_0(m_{01}, m_{02})}{\partial \theta_0} \right)^2 \right\rangle = \left(\tfrac{1}{2}\ell N_S\right)^2 \left\langle \left(\frac{m_{01}}{N_1} - \frac{m_{02}}{N_2} \right)^2 \right\rangle \quad , \tag{3.9}$$

where $N_k = S_k N_S + N_N/2$. With

$$\langle m_{0k}^2 \rangle \approx (N_k + 1) N_k \tag{3.10}$$

and

$$\langle m_{01}\, m_{02} \rangle = N_1 N_2 \quad , \tag{3.11}$$

the inequality (3.8) can be written as

$$\text{var } \phi_0^* \geqslant \frac{N_S + N_N}{N_S^2} \left[\ell^{-2} - \theta_0^2 \, \frac{N_S}{N_S + N_N} \right]^2 \quad . \tag{3.12}$$

Again neglecting θ_0 compared to $1/\ell$, the lower bound of the standard deviation is

$$\sigma_{0\,\min} = (N_S + N_N)^{1/2} / \ell N_S \quad . \tag{3.13}$$

This is the same as the beam-splitting formula, with the SNR now given by the ratio $N_S/(N_S + N_N)^{1/2}$. This suggests that the theoretical limit for the accuracy of the TAP derived from m_{01} and m_{02}, given N_S and N_N, depends on the shot noise generated by the target-returned laser illumination and the background radiation, and on the dark current. It should be noted that (3.13) applies also as a bound for the accuracy of angular position estimates for temporally noncoherent targets, for which M is large.

3.4 MAXIMUM LIKELIHOOD ESTIMATES OF TARGET ANGULAR POSITION

The theoretical bounds for the standard deviations of estimates of the TAP, such as those obtained above, do not identify the estimator whose standard deviation attains these bounds. The choice of the MLEs as good candidates for estimating the TAPs is made here because they are asymptotically efficient estimates; i.e., their variances attain the Cramér-Rao bounds as the number of statistically independent measurements increases.

3.4.1 MLE FOR FADING TARGET WITHOUT BACKGROUND ($1 \leqslant M < \infty$, $N_N = 0$)

The MLE of the TAP $\hat{\theta}_0$, is that value of θ_0 that is most likely to cause the observed values of n_1 and n_2 to occur. It maximizes the likelihood function $p(n_1, n_2 | \theta_0)$ for given n_1, n_2. If this maximum is interior to the range of θ_0 and the function is appropriately continuous, the MLE is found from the likelihood equation[25]

$$\partial p(n_1, n_2 | \theta_0)/\partial \theta_0 = 0 \quad . \tag{4.1}$$

By (2.5), (2.6) and the fact that θ_0 appears only in S_1, S_2,

$$\frac{\partial p}{\partial \theta_0} = \frac{\partial}{\partial \theta_0} \left\langle N^{n_1+n_2} e^{-N} \frac{S_1^{n_1}}{n_1!} \frac{S_2^{n_2}}{n_2!} \right\rangle = \frac{\left\langle N^{n_1+n_2} e^{-N} \right\rangle}{n_1! n_2!} \frac{\partial}{\partial \theta_0} \left(S_1^{n_1} S_2^{n_2} \right) = 0$$

and $\partial \left(S_1^{n_1} S_2^{n_2} \right) / \partial \theta_0$ is solved by

$$\hat{\theta}_0 = \ell^{-1} (n_1 - n_2) / (n_1 + n_2) \quad . \tag{4.2}$$

The processing required to realize the MLE of TAP requires taking the scaled ratio of the photocount difference to the total number of photocounts, where the scaling factor ℓ is known and depends on the shape of the PSF of the imaging telescope. This estimator is conceptually similar to the one employed in microwave angle-tracking monopulse systems.[9] In the event that both n_1 and n_2 are zero, it is intended that the processor not provide any TAP estimate at all, as if no light were incident.

The derivation of the mean and variance of the MLE of the TAP, $\hat{\theta}_0$, is presented in the appendix but the main results are stated and discussed here. The mean and variance of $\hat{\theta}_0$ are given by (A.9) and (A.18):

$$\langle \hat{\theta}_0 \rangle = \theta_0 (1 - J^{-M}) \tag{4.3}$$

and

$$\text{var } \hat{\theta}_0 = \ell^{-2} J^{-M} G + \theta_0^2 J^{-M} (1 - J^{-M} - G) \tag{4.4}$$

where

$$J = 1 + 1/\gamma = 1 + N_S/M \tag{4.5}$$

$$G = \ln J + \sum_{m=1}^{M-1} (J^m - 1)/m \quad . \tag{4.6}$$

For the strongest fading $(M = 1)$ the above equations can be rewritten in a form more useful for interpretation:

$$\langle \hat{\theta}_0 \rangle = \theta_0 N_S/(N_S + 1) \tag{4.7}$$

$$\text{var } \hat{\theta}_0 = \ell^{-2} (\ln N_p)/N_p - \theta_0^2 [(\ln N_p)/N_p - N_S/N_p^2] \tag{4.8}$$

$$\cong \ell^{-2} \frac{\ln(N_S + 1)}{N_S + 1} \quad , \tag{4.8a}$$

where $N_p = N_S + 1$ and the last form accounts for $\theta_0 \ll \ell^{-1}$.

Equations (4.3) and (4.7) show that the MLE of θ_0 is biased. This bias, which is known and can be corrected when N_S is known, decreases with increasing total signal N_S and approaches zero for large N_S. The rate of this convergence depends on the number of degrees of freedom M and increases as M increases. At the limiting case of large M (4.3) can be well approximated by

$$\langle \hat{\theta}_0 \rangle = \theta_0 (1 - e^{-N_S}) \quad . \tag{4.9}$$

For small signals and strong fading the bias cannot be disregarded. Figure 2 plots $\langle \hat{\theta}_0 \rangle / \theta_0$ as a function of N_S for different values of M. For $M = 1$ more than 50 signal photocounts are required to reduce the bias to the same extent as can just four signal counts for $M > 5$.

The variance of $\hat{\theta}_0$ can be written as a sum of terms dependent on and independent of the target position θ_0. Both terms of var $\hat{\theta}_0$ are dependent on the target fading and both can be made negligibly small for sufficiently large N_S. Figure 3 is a plot of the RMS error[29] $[\text{var } \hat{\theta}_0]^{1/2}$, in λ/D units, as a function of N_S for different values of M. The region covered is that of θ_0 small with respect to the diffraction angle λ/D. A square $D \times D$ pupil aperture was assumed for which $\ell = 2D/\lambda$. In the small photocount region $2 < N_S < 10$, target fading does not play a dominant role and the accuracy of $\hat{\theta}_0$ is limited by the signal shot noise. For larger N_S the limita-

tions imposed by target fading are clearly pronounced. An increase in the number of degrees of freedom M is particularly advantageous for fixed N_S when the fading is strong (M small).

Although θ_0 is biased, it is instructive to compare its standard deviation with the lower bound σ_{min} derived for unbiased estimates. The lower bound is plotted on Fig. 3 as a dashed line. From this comparison one concludes that for weak fading and for strong signals, for which the bias becomes negligible, σ_{min} can be used as a good approximation for determining the accuracy of $\hat{\theta}_0$. Figure 3 indicates that this approximation would be very poor for strong fading. Suppose that an RMS error no larger than 0.1 λ/D is desired. To achieve this accuracy the expected number of signal photocounts should be larger than 120 for $M = 1$ and larger than 25 for $M > 10$. Therefore, to obtain an accuracy of 0.1 λ/D, the required laser power must be five times larger for $M = 1$ than for $M > 10$.

In those instances when the bias is not negligible, the question of whether to modify the estimator to remove the bias can readily be treated by comparing the accuracies of both types of estimates, using the results presented here.

Several consequences for the design of illumination wavefronts and measurement schemes result from the above analysis of the variance of the MLE. Qualitatively, the target fading limitations can be decreased by decreasing the temporal coherence of illumination, as illustrated by the following three cases.

1. A stationary rough target is illuminated with a single pulse from a multiline laser. The illumination wavefront is a superposition of M laser lines mutually offset in frequency. The frequency offsets are assumed to be sufficiently large so that the speckle patterns at the receiver, each due to a single line, are mutually decorrelated.

2. A spinning target is illuminated with M short, equal-strength pulses from a single-line laser. The return from each pulse, rendered statistically independent from the others by the spin, is used to obtain a MLE of the TAP. All M estimates are used to obtain the sample mean of the estimates of the TAP. The RMS error of the sample mean is smaller than that of a single-pulse estimate by a factor of $M^{1/2}$.

3. A spinning target is illuminated with a long pulse from a single-line laser. During the integration time, which is not shorter than the pulse duration, let an average of M speckles be captured by the receiver aperture.

Cases 1 and 3 are formally similar: a single measurement is made, based on the photocounts generated by energy W with M degrees of freedom. In Case 2, M measurements are taken, each based on the photocounts generated by W with one degree of freedom. Combining Cases 1 and 3, by use of multiline radiation, one can perform a single measurement in which W is sensed with an effective degree of freedom equal to the product of those of the two cases. Combining Cases 1 and 2, by use of M pulses of M lines, M measurements are performed, each resulting from sensing W with M degrees

of freedom. All three cases and their combinations provide diversities instrumental in easing target-fading limitations.

Given that the total signal N_S is fixed in all three cases, is a smaller RMS error obtained from a single measurement with M degrees of freedom and N_S/M photocounts per degree of freedom (Cases 1 and 3) or from M measurements each based on N_S/M total photocounts with one degree of freedom (Case 2)? Generally, the RMS error of the MLE obtained from a single measurement, based on energy with M degrees of freedom, is smaller than the one obtained from M independent measurements, each based on energy with one degree of freedom, provided that other conditions are unchanged. In particular, this implies that measurements based on the long illumination pulse offer better results than the one based on averaging over many short pulses.

Two numerical examples are presented as an illustration of the use of the $\sigma_{MLE}(N_S,M)$ formula, based on (4.4).

Example 1: Let the total signal be $N_S = 100$. Dividing the signal equally among 10 laser lines that are sufficiently offset in frequency to produce 10 degrees of freedom in the energy deposited on the detector, we obtain an RMS error $\sigma_{MLE}(100,10) = 0.053\ \lambda/D$. If, instead, the total signal $N_S = 100$ is divided equally among 10 pulses, the RMS error of a single measurement is $\sigma_{MLE}(10,1) = 0.23\ \lambda/D$ and the RMS error obtained by averaging 10 measurements is $0.074\ \lambda/D$.

Example 2: For the same total signal $N_S = 100$ and dividing the signal equally among 5 laser lines, one obtains for the RMS error $\sigma_{MLE}(100,5) = 0.056\ \lambda/D$. The RMS error of the MLE obtained by averaging over 5 pulses each with signal $N_S = 20$ is $\sigma_{MLE}(20,1)/5^{1/2} = 0.085\ \lambda/D$.

In some situations, it may be simpler to replace the denominator of Eq. (4.2) by $\langle n_1 + n_2 \rangle$, an estimate of this expectation being obtained by averaging the total number of counts over many observations, each representing an independent realization of the process. The resulting estimator is not a MLE. It is expressed by:

$$\hat{\theta}_1 = \ell^{-1} \frac{n_1 - n_2}{\langle n_1 + n_2 \rangle} \quad . \tag{4.10}$$

Formally, the expectation in the denominator makes it statistically independent of the numerator. A similar situation occurs in microwave amplitude monopulse radars with slow AGC: the time period over which the denominator is averaged, the integration time, is long with respect to the inverse of the target scintillation bandwidth, so that the sum channel's fluctuations are eliminated while the difference channel remains stochastic. It has been found that the accuracy of tracking of microwave systems is limited by target scintillations (target fading) for slow AGC and free of these limitations for fast AGC.[26,27] Our results demonstrate that the same is true for optical systems, with $\hat{\theta}_1$ and $\hat{\theta}_0$ analogous to the estimators obtained in microwave monopulse radar with slow and fast

AGCs, respectively. The performance of $\hat{\theta}_1$, compared with that of $\hat{\theta}_0$, is discussed below.

The mean and variance of estimator θ_1 are

$$\langle \hat{\theta}_1 \rangle = (\ell d)^{-1} \langle n_1 - n_2 \rangle \tag{4.11}$$

$$\text{var } \hat{\theta}_1 = (\ell d)^{-2} \left[\sigma_{n1}^2 + \sigma_{n2}^2 - 2 \text{ cov}(n_1, n_2) \right] , \tag{4.12}$$

where $d = \langle n_1 + n_2 \rangle$, $\text{cov}(n_1, n_2)$ is the covariance of n_1 and n_2, and σ_{n1}^2 and σ_{n2}^2 are the variances of n_1 and n_2. The photocounts n_1 and n_2 obey the marginal PDFs $p(n_1)$, $p(n_2)$, which can be obtained from the joint one in Eq. (2.5) as

$$p(n_k) = \int_0^\infty dN p(N) \frac{(S_k N)^{n_k}}{n_k!} e^{-S_k N} . \tag{4.13}$$

The mean and the variance of n_k are given by[29]

$$\langle n_k \rangle = S_k N_S \tag{4.14}$$

$$\sigma_{nk}^2 = S_k N_S + S_k^2 N_S^2 / M \tag{4.15}$$

and the covariance is

$$\text{cov}(n_1, n_2) = S_1 S_2 N_S^2 / M . \tag{4.16}$$

Substituting these into (4.11, 4.12), yields the mean and variance of $\hat{\theta}_1$:

$$\langle \hat{\theta}_1 \rangle = \theta_0 \quad , \tag{4.17}$$

$$\text{var } \hat{\theta}_1 = \ell^{-2}/N_S + \theta_0^2/M \quad . \tag{4.18}$$

Thus, $\hat{\theta}_1$ is an unbiased estimator of θ_0. Its variance is a sum of two terms; the first depends on the PSF of the system (via ℓ) and is inversely proportional to the square of the signal-shot-noise-limited SNR. The second term is proportional to θ_0^2, and is inversely proportional to the square of the fading-limited SNR. For a target on the optical axis, $\theta_0 = 0$, the fading noise can be disregarded and the system performance is limited by the signal-shot-noise. For $\theta_0 \neq 0$ and large N_S the photocounting noise can be neglected with respect to the target-fading noise and the second term limits the accuracy of this estimator. For a fixed and nonzero value of θ_0, this term is largest for the deepest fading ($M = 1$). As M increases, the second term decreases and can be neglected at the limit of noncoherent light (large M).

Comparing the RMS error of $\hat{\theta}_0$ and $\hat{\theta}_1$ with the lower bound σ_{min} for the case of strong target-fading noise ($M = 1$, $\theta_0 = 0.1\ \lambda/D$), one concludes that (1) the theoretical limit for the RMS errors does not depend on the target fading, whereas the RMS erros of $\hat{\theta}_0$ and $\hat{\theta}_1$ are target noise dependent;

(2) the RMS error of $\hat{\theta}_1$, which is an unbiased estimate, is larger than σ_{min} for all values of signal; they are equal only if $\theta_0 = 0$ or if M is very large. The difference between them is negligible for small signals. For large signals the RMS error of $\hat{\theta}_1$ is significantly larger than σ_{min}, being three times larger than σ_{min} for $N_S = 10^3$ and a hundred times larger for $N_S = 10^4$; (3) the estimate $\hat{\theta}_0$ is biased, which allows its RMS error to be smaller than σ_{min} for small signals. For $N_S = 1$, for example, for which the bias of $\hat{\theta}_0$ is 50 per cent, the RMS error of $\hat{\theta}_0$ and σ_{min} are 0.3 λ/D and 0.5 λ/D, respectively. The RMS error of $\hat{\theta}_0$ is larger than that of $\hat{\theta}_1$ for values of N_S for which $\hat{\theta}_0$ is approximately unbiased and signal shot noise dominates. As the signal increases to where the target-fading noise dominates, $\hat{\theta}_0$ performs significantly better than $\hat{\theta}_1$: the RMS errors of $\hat{\theta}_0$ are 2.4 and 6.6 times smaller than the corresponding values for $\hat{\theta}_1$ for $N_S = 10^3$ and $N_S = 10^4$, respectively.

3.4.2 MLE for Fading Target in Weak Background Noise

In the preceding section the background noise and dark current were neglected in the derivation of the MLE of the TAP. For low levels of signal light, however, the analysis ought to include such noise. This is considered in this section under the assumption that the noise is weak: $N_N < 1$, $(N_N/N_S) \ll 1$. The mean and variance of the MLE, $\hat{\Lambda}_0$, are computed for $M = 1$. The accuracy of $\hat{\Lambda}_0$ for intermediate values of M is also

discussed, based on computer-simulated data. Confidence in the simulations is gained from their good agreement with the analytically derived formulas for $M = 1$ and $M = \infty$.

The MLE is the value of θ_0 that maximizes $q_1(m_1, m_2)$ given in (2.9). Differentiation yields the condition

$$\left(\frac{m_1}{S_1} - \frac{m_2}{S_2}\right)(1 - N_N) + \left[\frac{m_1(m_1 - 1)}{S_1^2} - \frac{m_2(m_2 - 1)}{S_2^2}\right]\frac{N_N}{2N_M} = 0 \quad . \tag{4.19}$$

But to zero order in the noise N_N,

$$\frac{m_1}{S_1} = \frac{m_2}{S_2} = m_1 + m_2 \quad .$$

Applying these equations to the factor of N_N in (4.19), the maximum likelihood condition becomes, to first order in N_N,

$$m_1 S_2 - m_2 S_1 = (m_1 - m_2)N_N/2N_M \quad . \tag{4.19a}$$

Combining this with (2.3a) and (2.3b), one finds that the noiseless MLE is modified by the factor $1 + N_N/N_M$:

$$\hat{\Lambda}_0 = \ell^{-1}\,\frac{m_1 - m_2}{m_1 + m_2}\left[1 + \frac{N_N}{N_S}\,\frac{M + N_S}{M - 1 + m_1 + m_2}\right] \quad . \tag{4.20}$$

To realize $\hat{\Lambda}_0$ it is necessary to know N_S, N_N and M. These parameters are assumed to be known from averaging of many independent measurements, of the background alone to obtain an estimate of N_N, of the target-returned laser illumination with the background to obtain estimates of the sum $N_S + N_N$, and

lastly of the variance of the total number of photocounts, $\mathrm{var}(m_1 + m_2)$. All these estimates are needed to estimate M as

$$M = N_S^2 [\mathrm{var}(m_1 + m_2) - (N_S + N_N)]^{-1} \quad , \tag{4.21}$$

since $\mathrm{var}(m_1 + m_2) = N_S + N_N + \mathrm{var}\ N$ and $\mathrm{var}\ N = N_S^2/M$.

To calculate the mean and variance of $\hat{\Lambda}_0$ it is convenient to introduce the following notation,

$$\hat{\Lambda}_0 = \Lambda_S + \Lambda_N \quad , \tag{4.22}$$

$$q_1(m_1, m_2) = \langle (Q_S + Q_N)\, e^{-N} \rangle \quad , \tag{4.23}$$

where subscripts S and N are used to indicate terms that are independent and dependent on the background noise, respectively, and the expectation is with respect to N; i.e.,

$$\Lambda_S = \Lambda_S(m_1, m_2) = \ell^{-1} \frac{m_1 - m_2}{m_1 + m_2} \quad ,$$

$$\Lambda_N = N_N (1 + M/N_S) \Lambda_S(m_1, m_2)/(M - 1 + m_1 + m_2) \quad ,$$

$$Q_S(m_1, m_2) = \frac{(S_1 N)^{m_1}}{m_1!} \frac{(S_2 N)^{m_2}}{m_2!} \quad ,$$

$$Q_N = N_N [\tfrac{1}{2} Q_S(m_1, m_2 - 1) + \tfrac{1}{2} Q_S(m_1 - 1, m_2) - Q_S(m_1, m_2)] \quad .$$

The approximate expressions for the mean and variance of $\hat{\Lambda}_0$, to first order in N_N/N_S, are

$$\langle \hat{\Lambda}_0 \rangle = \langle \hat{\theta}_0 \rangle + \langle e^{-N} \sum (Q_S \Lambda_N + Q_N \Lambda_S) \rangle \quad , \tag{4.24}$$

$$\text{var } \hat{\Lambda}_0 = \text{var } \hat{\theta}_0 + \langle e^{-N} \sum Q_N \Lambda_S (\Lambda_S - 2\langle \hat{\theta}_0 \rangle) \rangle + 2 \langle e^{-N} \sum Q_S (\Lambda_S - \langle \hat{\theta}_0 \rangle) \Lambda_N \rangle \tag{4.25}$$

where the sums are over m_1 and m_2, exclusive of $m_1 = m_2 = 0$, the expectations are taken over N, and $\langle \hat{\theta}_0 \rangle$ and var $\hat{\theta}_0$ were computed in Sec. (3.4.1). The remaining terms in (4.24-25) can be evaluated by extension of the computational techniques employed in the Appendix. The expressions involve modified exponential integrals and are not informative in general. For M = 1, however, the analytic expression for the mean of the estimator,

$$\langle \hat{\Lambda}_0 \rangle = \theta_0 (N_S + N_N)/(N_S + 1) \quad , \tag{4.26}$$

valid for N_N smaller than both N_S and unity, shows that the noise, when weak, reduces the bias of the MLE, because the noise and signal bias act in opposite directions.

Standard deviations of the MLE $\hat{\Lambda}_0$ were obtained in computer simulations using 5000 realizations of the random m_1 and m_2 and examined as functions of the signal N_S for different values of M and N_N. For large N_S, the RMS error of $\hat{\Lambda}_0$ can be considered practically equal to that of $\hat{\theta}_0$. For weak signals, however, the difference between the errors of these estimators can be appreciable. The percentage difference between the RMS errors of $\hat{\Lambda}_0$ and $\hat{\theta}_0$, normalized to that of $\hat{\theta}_0$, is plotted in Fig. 4 as a function of the signal N_S, for $M = 1,2,20$, and for $N_N = 0.1$ (solid lines) and $N_N = 0.5$ (dashed lines). The RMS error of $\hat{\Lambda}_0$ is larger than that of $\hat{\theta}_0$ for the same N_S, and M. The normalized error difference decreases with the signal N_S and, for fixed N_S and N_N, decreases with M. Also, for fixed M and N_S, it increases with the noise level.

Consider now an estimator $\hat{\Lambda}_1$ realizable with a slow AGC system. This estimator is defined as:

$$\hat{\Lambda}_1 = \ell^{-1} \left\langle \frac{m_1 - m_2}{m_1 + m_2} \right\rangle \left(1 + \frac{N_N}{N_S} \frac{M + N_S}{M - 1 + \langle m_2 + m_2 \rangle} \right) \quad . \tag{4.27}$$

The mean and variance of $\hat{\Lambda}_1$ are readily obtained from those of $m_1 \pm m_2$ from (2.8), without approximation.

$$\langle \hat{\Lambda}_1 \rangle = \theta_0 (N_S + XN_N)/(N_S + N_N) \quad , \tag{4.28}$$

$$\text{var } \hat{\Lambda}_1 = \left[\frac{\theta_0^2}{M} + \ell^{-2} \frac{N_S + N_N}{N_S^2} \right] \left[\frac{N_S + XN_N}{N_S + N_N} \right]^2 \quad , \tag{4.29}$$

where $X = (N_S + M)/(N_S + M + N_N - 1)$. This estimator is biased, except for $N_N = 1$. Its RMS error is target-fading limited for large signals.

3.4.3 MLE FOR A NONFADING TARGET IN BACKGROUND NOISE $(M \to \infty,\ N_N > 0)$

The likelihood function for this case is $q_0(m_{01}, m_{02} | N_S)$, as in (2.7a), and the MLE is most easily obtained by maximizing $\ln q_0$. This estimator is

$$\hat{\phi}_0 = \ell^{-1}\left(1 + \frac{N_N}{N_S}\right)\frac{m_{01} - m_{02}}{m_{01} + m_{02}} \quad . \tag{4.30}$$

The mean and variance of $\hat{\phi}_0$ can be obtained by the method used in the Appendix.

$$\langle \hat{\phi}_0 \rangle = \theta_0\left[1 - e^{-N_T}\right] \quad , \tag{4.31}$$

$$\text{var}\ \hat{\phi}_0 = \theta_0^2 e^{-N_T}\left[1 - e^{-N_T} + \text{Ein}(-N_T)\right] - \ell^{-2}(N_T/N_S)^2 e^{-N_T}\ \text{Ein}(-N_T) \quad , \tag{4.32}$$

where $N_T = N_S + N_N$ and the exponential integral is the one that appears in (A-13). The MLE is biased, but underestimates θ_0 only slightly whenever the total of signal and noise is not negligible. In this case the RMS error in $\hat{\phi}_0$ can be considered equal to the lower bound $\sigma_{0\,\min}$ for all practical purposes.

Finally, consider an estimate $\hat{\phi}_1$, defined as

$$\hat{\phi}_1 = \ell^{-1} \frac{N_T}{N_S} \left\langle \frac{m_{01} - m_{02}}{m_{01} + m_{02}} \right\rangle \quad . \tag{4.33}$$

From the mean and variance of $m_{01} \pm m_{02}$, there follows that

$$\langle \hat{\phi}_1 \rangle = \theta_0 \tag{4.34}$$

$$\text{var } \hat{\phi}_1 = \ell^{-2} (N_S + N_N)/N_S^2 \quad . \tag{4.35}$$

Thus, this estimator is unbiased and its standard deviation equals the lower bound $\sigma_{0\,\min}$.

3.5 SUMMARY

In a laser radar monopulse system, the angular position of a target is estimated by measuring the location of the target's photocounting image by means of a noncoherent four-quadrant detector. The limitations imposed by target fading and by signal and background shot and dark current noise on the accuracy of the estimate have been investigated. The theoretical limits given by the Cramér-Rao lower bounds for the standard deviations of the estimates have been derived for fading and nonfading targets. For several cases it has been shown that the lower bounds are given by the beam-splitting formula; i.e., that the standard deviations are proportional to the diffraction-limited angular resolution of the imaging telescope and inversely proportional to the SNR, where the noise includes the shot noise generated by the target and background radiation and dark current, and do not depend on the target fading.

Maximum likelihood estimates have been derived for fading and nonfading targets and their means and standard deviations have been evaluated. All these estimates share the following properties:

1. They depend on the familiar monopulse ratio which, for the photocounting problem, is given by the ratio of the

difference of the total number of photocounts at the detector outputs to their sum. This normalization makes the angular measurement independent of the target range and significantly reduces the impact of target fading on its accuracy.

2. They are biased. For nonfluctuating targets, the bias decreases exponentially with the signal and background noise. For fading targets the bias depends on the number of degrees of freedom, M, and decreases monotonically with the signal at a rate that is significantly faster for $M > 5$ than for $M = 1$. For $M > 5$ and $N_S > 2$, the estimates for fluctuating targets can be considered practically unbiased.

3. The standard deviations of the estimates approach the theoretical Cramér-Rao limits for unbiased estimates when the signals are large enough to make the MLEs unbiased.

4. The processing of data according to the MLEs requires systems with fast automatic gain control, which can follow the temporal fluctuations of the target fading. The fast AGC is necessary to obtain the correlation between the difference and sum channels. If the AGC is slow, the difference and sum photocounts are decorrelated and the corresponding estimates, although unbiased, have standard deviations that are limited for large signals by target fading noise.

3.6 APPENDIX: MEAN AND VARIANCE OF MLE

We need $\langle r \rangle$ and $\langle r^2 \rangle$ for

$$r = \frac{n_1 - n_2}{n_1 + n_2} \quad , \tag{A.1}$$

where the counts n_1, n_2 are doubly stochastic:

$$\langle r^s \rangle = \int_0^\infty \sum_{n_1, n_2} r^s \, p(n_1, n_2 | N) p(N) dN \tag{A.2}$$

with

$$p(n_1, n_2 | N) = \frac{(S_1 N)^{n_1}}{n_1!} \frac{(S_2 N)^{n_2}}{n_2!} e^{-N} \tag{A.3}$$

and

$$p(N) = \gamma^M \frac{N^{M-1}}{(M-1)!} e^{-\gamma N} \quad . \tag{A.4}$$

The sum in (A.2) must exclude the possibility of no counts at all, $n_1 = n_2 = 0$. Let,

$$H(x, S_1, S_2) = \sum_{n_1, n_2} \frac{n_1 - n_2}{n_1 + n_2} x^{n_1 + n_2} \frac{S_1^{n_1}}{n_1!} \frac{S_2^{n_2}}{n_2!} \quad . \tag{A.5}$$

Then

$$x \partial H / \partial x = \sum_{n_1, n_2} (n_1 - n_2) \frac{(x S_1)^{n_1}}{n_1!} \frac{(x S_2)^{n_2}}{n_2!} \quad , \tag{A.6}$$

which readily sums to

$$x\partial H/\partial x = x(S_1 - S_2)\, e^{(S_1+S_2)x} = x(S_1 - S_2)e^x \qquad (A.7)$$

since $S_1 + S_2 = 1$. Integrating this, with $H(0,S_1,S_2) = 0$, yields

$$H(x,S_1,S_2) = (S_1 - S_2)(e^x - 1) \quad . \qquad (A.8)$$

It follows that, setting $J = 1 + 1/\gamma$,

$$\begin{aligned} \langle r \rangle &= \int_0^\infty H(N,S_1,S_2)\; e^{-N} p(N) dN \\ &= (S_1 - S_2)\,\langle 1 - e^{-N} \rangle \qquad (A.9) \\ &= (S_1 - S_2)\,(1 - J^{-M}) \end{aligned}$$

by use of (A.4)

Similarly, to obtain the variance, evaluate

$$K(x,S_1,S_2) = \sum_{n_1,n_2} \left(\frac{n_1 - n_2}{n_1 + n_2}\right)^2 x^{n_1+n_2}\, \frac{S_1^{n_1}}{n_1!}\, \frac{S_2^{n_2}}{n_2!} \qquad (A.10)$$

by forming

$$x\, \frac{\partial}{\partial x}\left(x\, \frac{\partial K}{\partial x}\right) = \sum_{n_1,n_2} (n_1 - n_2)^2 \frac{(xS_1)^{n_1}}{n_1!}\, \frac{(xS_2)^{n_2}}{n_2!} \qquad (A.11)$$

which, after rewriting $(n_1 - n_2)^2$ as $[n_1(n_1 - 1) + n_1 - 2n_1n_2 + n_2(n_2 - 1) + n_2]$, readily sums to

$$x \frac{\partial}{\partial x}\left(x \frac{\partial K}{\partial x}\right) = (x^2 S_1^2 + xS_1 - 2x^2 S_1 S_2 + x^2 S_2^2 + xS_2)e^x$$
$$= [x^2 (S_1 - S_2)^2 + x]e^x \quad . \tag{A.12}$$

Integrating twice yields K in terms of the exponential integral:

$$K(x, S_1, S_2) = [1 - (S_1 - S_2)^2] \int_0^x \frac{e^u - 1}{u}\, du + (e^x - 1)(S_1 - S_2)^2$$
$$= 4S_1 S_2[-Ein(-x)] + (S_1 - S_2)^2 (e^x - 1) \quad . \tag{A.13}$$

Thus,

$$\langle r^2 \rangle = \int_0^N K(N, S_1, S_2) e^{-N} p(N) dN$$
$$= 4S_1 S_2 \langle -e^{-N}\, Ein(-N) \rangle + (S_1 - S_2)^2 \langle 1 - e^{-N} \rangle \quad . \tag{A.14}$$

The double integral for the expectation involving the exponential integral can be evaluated as follows:

$$\langle -e^{-N}\, Ein(-N) \rangle = \int_0^\infty dN p(N) e^{-N} \int_0^N \frac{e^x - 1}{x}\, dx$$
$$= \int_0^\infty dx\, \frac{e^x - 1}{x} \int_x^\infty dN p(N) e^{-N}$$
$$= \left(\frac{\gamma}{1+\gamma}\right)^M \sum_{m=0}^{M-1} \frac{(1+\gamma)^m}{m!} \int_0^\infty dx\, x^{m-1} \left[\exp(-\gamma x) - \exp(-[1+\gamma]x)\right]$$
$$= \left(\frac{\gamma}{1+\gamma}\right)^M \left[\ln\left(1 + \frac{1}{\gamma}\right) + \sum_{m=1}^{M-1} \frac{(1 + \frac{1}{\gamma})^m - 1}{m}\right] \quad . \tag{A.15}$$

Hence, with $J = 1 + 1/\gamma$,

$$\text{var } r = 4S_1S_2J^{-M}\left[\ln J + \sum_{m=1}^{M-1}\frac{J^m - 1}{m}\right] + (S_1 - S_2)^2J^{-M}(1 - J^{-M}) \qquad (A.16)$$

or, since $4S_1S_2 = 1 - (S_1 - S_2)^2$ and letting

$$G = \ln J + \sum_{m=1}^{M-1}(J^m - 1)/m \quad , \qquad (A.17)$$

$$\text{var } r = J^{-M}G + (S_1 - S_2)^2J^{-M}(1 - J^{-M} - G) \quad . \qquad (A.18)$$

3.7 References

1. J. Flom, Appl. Opt., 11, 291 (1972).
2. B. E. M. Saleh, Appl. Opt., 13, 1824 (1974).
3. T. P. McGarty, IEEE Trans. Aerosp. and Electron. Syst., AES-5, 1974 (1969).
4. J. Amoss and F. Davidson, Appl. Opt., 11, 1793 (1972).
5. C. W. Helstrom, J. Opt. Soc. Am., 62, 416 (1972).
6. C. W. Helstrom, L. Wang, IEEE Trans. Aerosp. and Electron., AES-9, 561 (1973).
7. C. McIntyre, W. N. Peters, C. Chi, and H. E. Wischnia, Proc. IEEE, 58, 1491 (1970).
8. D. R. Rhodes, "Introduction to Monopulse," (McGraw-Hill, New York, 1959).
9. K. D. Barton, "Radar System Analysis," (Prentice-Hall, Inc., Englewood Cliffs, New Jersey, 1964), pp. 263-315.
10. M. Elbaum, M. King, W. Edelson and P. Diament, J. Opt. Soc. Am., 65A, 1204 (1975).
11. J. W. Goodman, in "Remote Techniques for Capillary Wave Measurement," ed. by K. S. Krishnan and N. A. Peppers (Stanford Research Inst. Rep., Stanford, Calif., 1973).
12. M. Elbaum and P. Diament, Appl. Opt., 15, 2268 (1976).

13. J. W. Goodman, "Statistical Properties of Laser Speckle and Related Phenomena," in "Laser Speckle and Related Phenomena," ed. by J. C. Dainty (Springer Verlag, Berlin Heidelberg New York, 1975), Vol. 9, Applied Physics.

14. M. Born, E. Wolf, "Principle of Optics," 4th ed. (Pergamon Press, London, 1970).

15. H. Cramér, "Mathematical Methods of Statistics," (Princeton University Press, Princeton, N.J., 1957).

16. M. Elbaum, P. Diament and M. King, J. Opt. Soc. Am., 65A, 1198 (1975).

17. M. C. Teich, "Coherent Detection in the Infrared," in "Semiconductors and Semimetals," edited by R. K. Willardson and A. C. Beer (Academic Press, New York, 1970), Vol. 5, Infrared Detectors.

18. L. Mandel, Proc. Phys. Soc., 74, 233 (1959).

19. L. Mandel, J. Opt. Soc. Am., 51, 1342 (1961).

20. J. W. Goodman, Proc. IEEE, 53, 1688 (1965).

21. W. Pratt, "Laser Communication Systems," (John Wiley and Sons, Inc., New York, 1969).

22. J. W. Goodman, Stanford Electronics Laboratory Report, Stanford, Calif. (1963).

23. M. Elbaum, M. Greenebaum and M. King, Opt. Commun., 5, 171 (1972).

24. A. J. Thomasian, "The Structure of Probability Theory with Applications," (McGraw-Hill Book Company, New York, 1969).

25. H. L. Van Trees, "Detection, Estimation, and Modulation Theory – Part 1," (John Wiley and Sons, Inc., New York, 1969).

26. J. H. Dunn and D. D. Howard, Proc. IRE, 47, 430 (1959).

27. J. H. Dunn, D. D. Howard and A. M. King, Proc. IRE, 47, 855 (1959).

28. J. Perina, "Coherence of Light," (Van Nostrand Reinhold Company, Ltd., London, 1971).

29. The standard deviation of the estimates is used herein as the RMS error, in the sense of uncertainty of measurement, because the biases are considered known. The authors are grateful to one of the reviewers for calling attention to the distinction in terminology regarding biased estimators.

3.8 Figure Captions

Fig. 1. Single-Axis tracking sensor. L = laser, O = object, T = telescope, Q = four-quadrant prism, R = receiver irradiance, I = image irradiance, n_1, n_2 = output photocounts. The areas under the irradiance curve on the two sides of the center line are in the ratio $S_1 : S_2$.

Fig. 2. Normalized mean of MLE $\hat{\theta}_0$ vs mean signal count.

Fig. 3. RMS error of MLE $\hat{\theta}_0$ vs mean signal count. The dashed line is the Cramér-Rao lower bound.

Fig. 4. Normalized difference between RMS errors of $\hat{\Lambda}_0$ and $\hat{\theta}_0$: $100(\sigma_\Lambda - \sigma_\theta)/\sigma_\theta$ vs mean signal count for noise counts $N_N = 0.1$ (solid lines) and $N_N = 0.5$ (dashed lines).

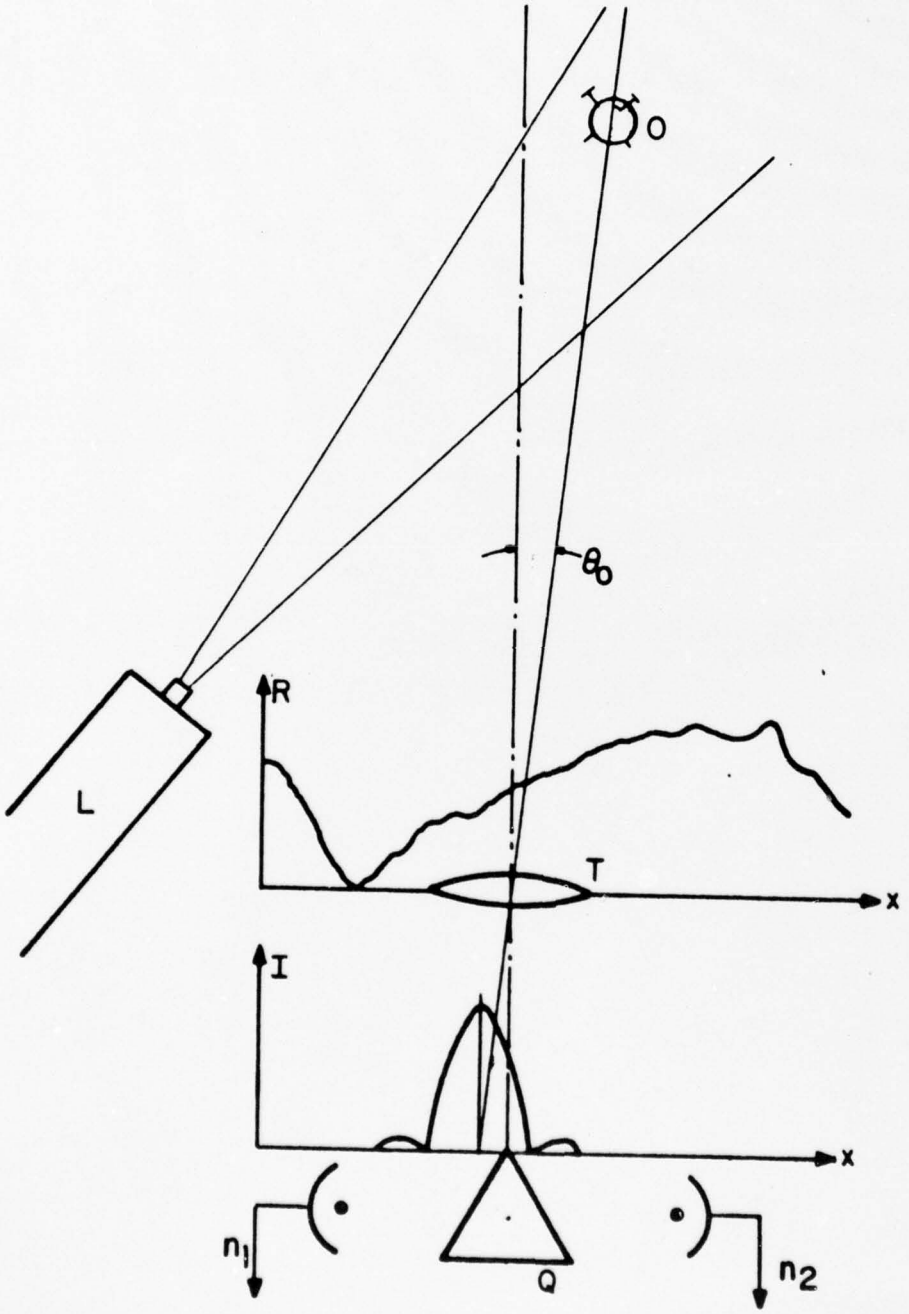

Fig. 1

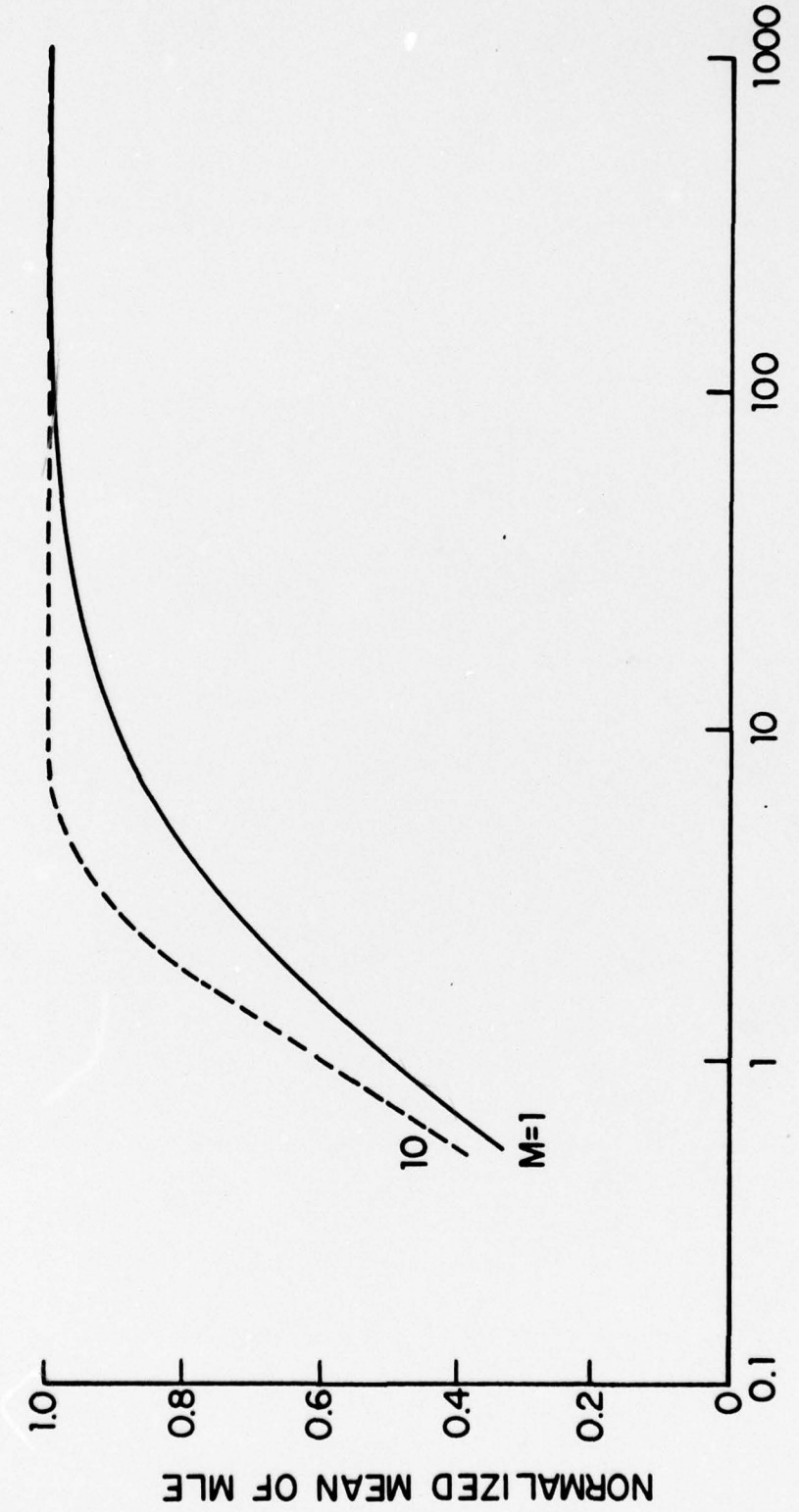
NORMALIZED MEAN OF MLE
1.0
0.8
0.6
0.4
0.2
0
0.1
1
10
100
1000
MEAN SIGNAL PHOTOCOUNT (N_S)
M=1
10

Fig. 2

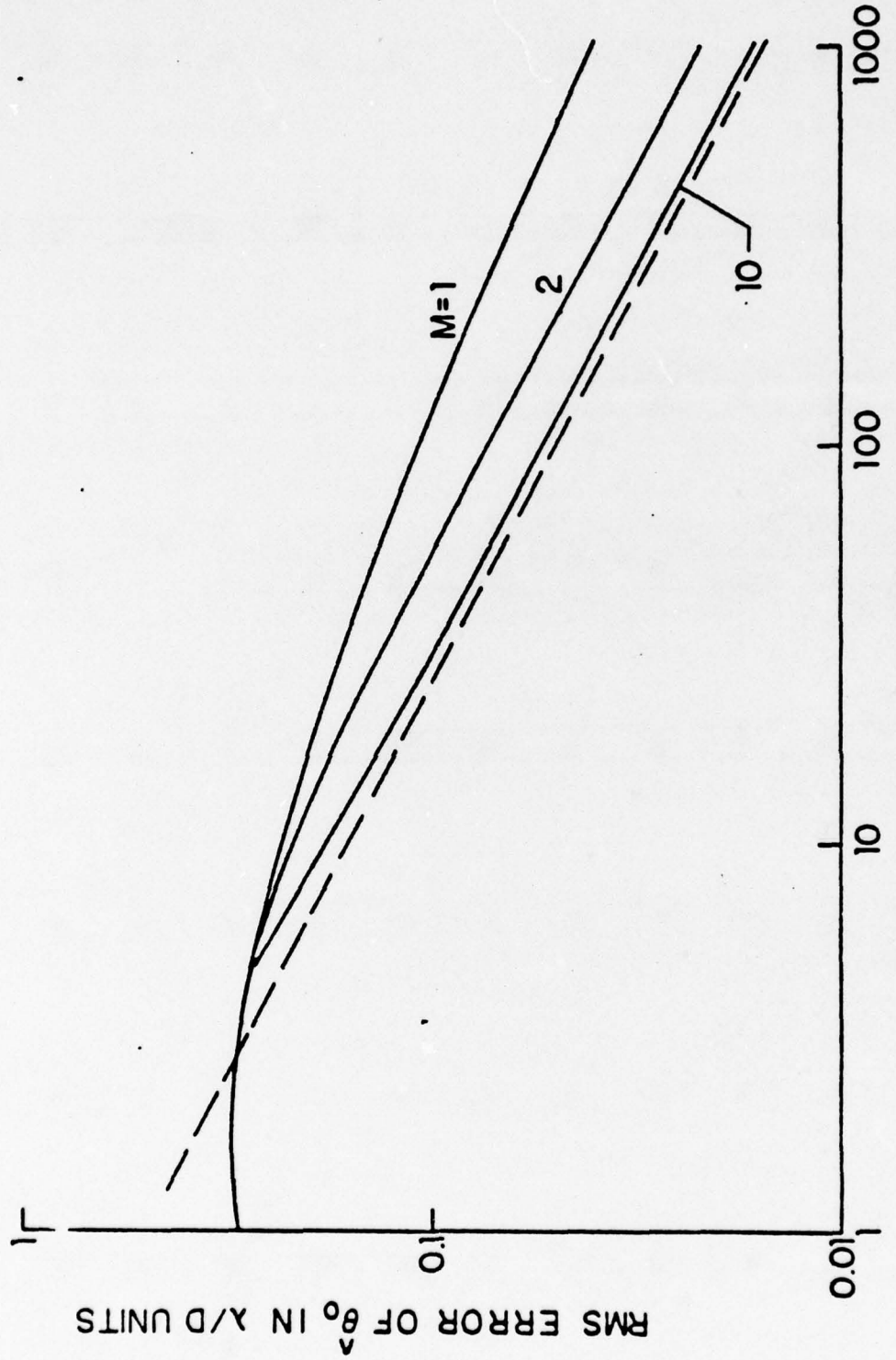
M=1
2
10
1000
100
10
1
0.1
0.01
MEAN SIGNAL PHOTOCOUNT (N_s)
RMS ERROR OF $\hat{\theta}_o$ IN λ/D UNITS

Fig. 3

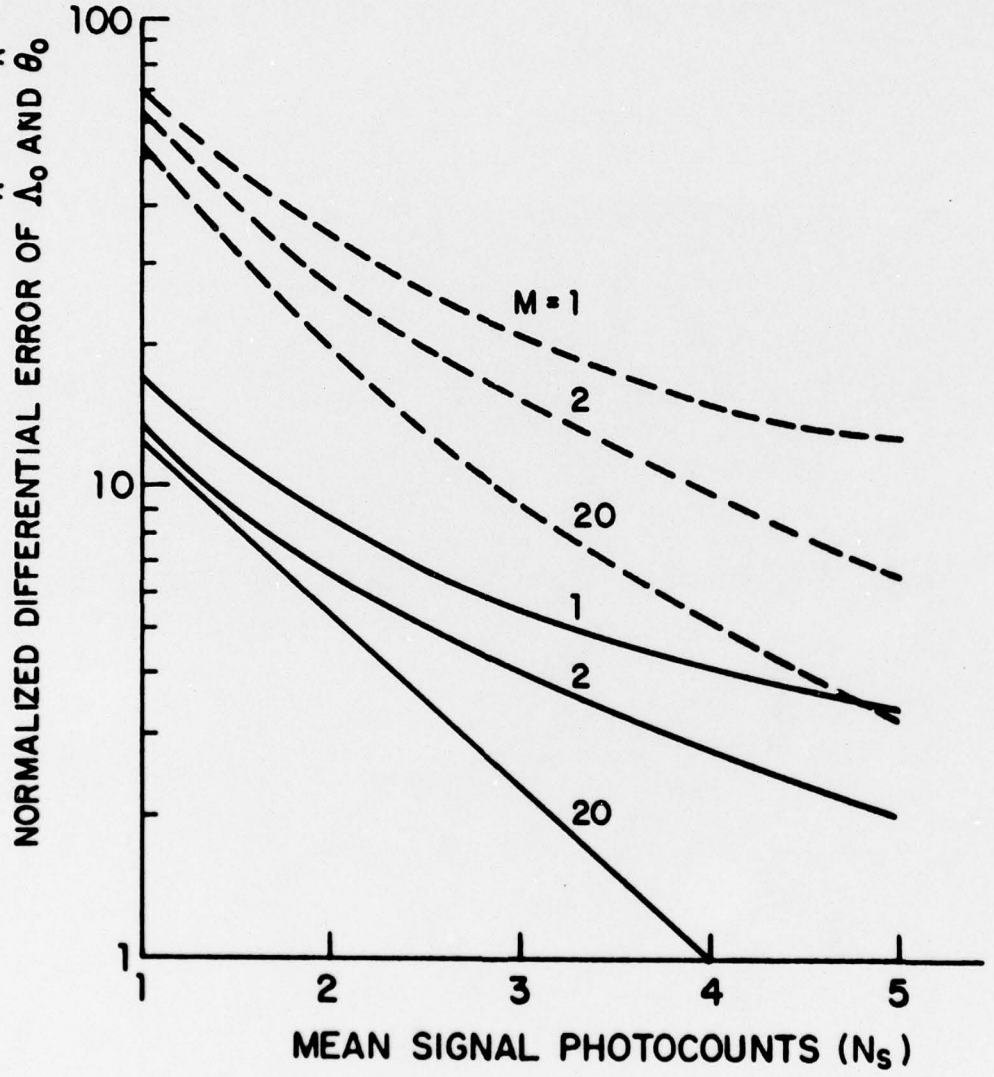
100
10
1
NORMALIZED DIFFERENTIAL ERROR OF $\hat{A}_0$ AND $\hat{\theta}_0$
M = 1
2
20
1
2
20
1
2
3
4
5
MEAN SIGNAL PHOTOCOUNTS (N_S)

Fig. 4

IV. ESTIMATION OF IMAGE CENTROID, SIZE, AND ORIENTATION WITH LASER RADAR

Angular tracking of targets with monopulse laser radar can be performed by tracking the centroid of the image. The image irradiance distribution is sensed with an array of noncoherent photocounting detectors and the individual counts processed to provide estimates of the image centroid coordinates and of its size and orientation. These estimates are discussed for optically rough and smooth extended targets, viewed against a noncoherent uniform background. General expressions for the mean and variance of the image centroid and second moment are obtained as a function of coherence of illumination, target extent, number of degrees of freedom in the target's image, the diffraction-limited resolution of the image telescope, and the integration time of the detectors. The fundamental limits imposed on the accuracy of the estimates by the shot noise from the image and background irradiances and by the laser speckle noise are discussed.

Portions of these results were presented at the 1975 meeting of the Opt. Soc. of Amer. in Boston, J. Opt. Soc. Amer., 61, 1204A.
Submitted for publication in Appl. Optics with P. Diament.

4.1 Introduction

An important application of laser radar is to angular tracking, in which a sequence of direct measurements of target position is fed into a tracking filter to produce refined estimates of present and future target position. The theory of angular tracking developed for microwave radars[1,2] does not apply fully to laser radars. Unlike microwave radars, laser systems can resolve targets with only modest-size telescope apertures. The quantum noise may be quite apparent in the optical electromagnetic spectrum. If background radiation noise is not a dominant factor, the laser energy returned by the target can be reliably sensed with noncoherent detectors. These are simpler than heterodyne sensors and are particularly attractive for use with recently developed powerful chemical laser sources that have poor temporal coherence.

This paper discusses estimation of angular position, size, and orientation of extended targets by use of monopulse laser radars which derive their information about target angular position (TAP) and target size and orientation (TSO) from a single pulse. The TAP is estimated from the position of the centroid of the image. The image centroid, one of many ad hoc estimators that can be used for TAP estimation, generalizes to extended targets

the usual[3] point target[4] angular estimators derived from four-quadrant image sensing detectors. The TSO is estimated from the properly normalized image second-moment tensor.

The imaging system receives both reflected light from the target, which is illuminated with the laser beam provided for tracking, and from uniform, noncoherent background radiation. This light is imaged onto the detector array, which converts the photon flow into an image photocounting distribution (IPD), the electrical signal used by the image processor. The image processor is to estimate accurately the image position, size and orientation from each received pulse.

The sensor consists of an array of L detectors; the k-th one is located at position $\underset{\sim}{r}_k$ and registers m_k photoelectron counts in response to one laser pulse. Of these, some are background photoelectrons and dark current electrons, the rest are signal photoelectrons. In the absence of a target image, the noise count consists of only background and dark current, fluctuating in number about a mean noise count $\langle m_N \rangle$ that is assumed to be known and the same for all the detectors. The reduced count at the k-th detector is

$$n_k = m_k - \langle m_N \rangle \quad , \tag{1}$$

the total count diminished by the known mean noise count; this includes the random signal counts and the fluctuations of the noise counts.

The processor considered here provides the tracking system with the location of the reduced IPD centroid and second moment. The former is the vector (see Fig. 1)

$$\underset{\sim}{c} = \sum \underset{\sim}{r}_k n_k / \sum n_\ell \qquad (2)$$

and the latter is the optical moment of inertia tensor

$$\underset{\sim}{I} = \sum \underset{\sim}{r}_k \underset{\sim}{r}_k n_k / \sum n_\ell \quad . \qquad (3)$$

The summations are over all the detectors of the array. The moments are measured with respect to the optical axis of the imaging system. Upon shifting $\underset{\sim}{I}$ to refer to the optical centroid, its eigenvalues and eigenvectors provide the image size and orientation.

The numerators of these quantities estimate the first and second moments of the image irradiance distribution and, except for their randomness, correspond to those of the irradiance distribution at the target. The normalization denominator for both moments is the total number of counts in the array, reduced by the expected value of the total number of noise counts. This normalization factor makes the position, size, and orientation measurements independent of the target's range and, because it too is random, can ease the dependence of the measured moments on the target-related random fluctuations, provided a correlation exists between the total count and each of the moments.

The statistical properties of the estimators depend on those of the IPD. It is assumed that the noise counts obey Poisson statistics with parameter equal to the sum of the mean background and dark current counts and are independent of each other and of the signal counts. The statistics of the signal counts reflect those of the energy W_k deposited on the individual detectors by the laser field returned from the target. These counts are generally correlated.

As has been shown,[5] the statistical properties of the energy at each detector depend on the coherence of the illuminating light, the target-surface roughness, the width of the telescope point-spread functions, the illuminator-target-telescope geometry, and the aperture and integration time of the detector. The random fluctuations in W make the resultant signal counts a doubly stochastic Poisson process.[6] For an optically rough target, the returned field is a stochastic spatio-temporal, zero-mean complex Gaussian process and the photoelectron counts obey a negative binomial distribution with M degrees of freedom.[5,7] The image irradiance distribution from such fields has the characteristic random spatial structure referred to as the laser speckle pattern.[8,9] For an optically smooth target and temporally coherent illumination, the image field does not fluctuate and the photoelectrons are then only singly stochastic, obeying Poisson statistics.[5,7]

To determine the limitations imposed on the accuracies of the estimators by the laser speckle structure, the signal and background shot noise and the dark current, the general expressions for the means and variances of $\underset{\sim}{c}$ and $\underset{\sim}{I}$ are derived in the next section. The relevant expressions are specialized in Sec. 4.3 for TAP estimation with the monopulse laser.

4.2 MEAN AND VARIANCE OF THE ESTIMATORS

The performance and accuracy of the estimators $\underset{\sim}{c}$ and $\underset{\sim}{I}$ are determined by their means and covariance matrices. These can be evaluated by adapting the method of statistical error propagation[10] or the delta method[11] to the centroid[12] and second moment expressions. It is shown that the means and variances for both estimators are expressible in terms of a detection matrix comprised of the covariances of pairs of counts,

$$\mu_{k\ell} = \langle [m_k - \langle m_k \rangle][m_\ell - \langle m_\ell \rangle] \rangle \quad . \tag{4}$$

Both moments, as well as higher-order ones that could be treated analogously, are of the form of a deterministic function Φ_k of the location of the k-th detector, averaged over the reduced counts at each detector:

$$E = \sum \Phi_k n_k / \sum n_\ell \quad . \tag{5}$$

This random quantity is intended to estimate the corresponding property of the image

$$F = \sum \Phi_k \langle n_k \rangle / \sum \langle n_\ell \rangle \quad . \tag{6}$$

The quantity Φ_k, and hence also E and F, can be of any scalar, vector, or tensor character. For the centroid, Φ_k is

$\underset{\sim}{r}_k$, E is $\underset{\sim}{\varsigma}$, and F is the true image centroid $\underset{\sim}{s}$. For the second moment tensor, Φ_k is $\underset{\sim}{r}_k\underset{\sim}{r}_k$, E is $\underset{\sim}{I}$, and F is the true optical moment of inertia tensor $\underset{\sim}{M}$, referred to the optical axis.

Let $N = \sum\langle n_k\rangle$ be the total mean reduced count and let $\Delta x = x - \langle x\rangle$ be the deviation from its mean of any random variable x. When expressed in terms of such deviations, the estimator is

$$E = (F + \sum \Phi_k \Delta n_k / N)/(1 + \sum \Delta n_\ell / N) \quad . \tag{7}$$

Expanding the reciprocal of the denominator in a Taylor series and retaining terms to only the second order in Δn,

$$E = F + \sum_k (\Phi_k - F)\Delta n_k / N - \sum_{k,\ell} (\Phi_k - F)\Delta n_k \Delta n_\ell / N^2 \quad . \tag{8}$$

It follows that the mean of the estimator is, to this order,

$$\langle E\rangle = F - \sum_{k,\ell} (\Phi_k - F)\langle \Delta n_k \Delta n_\ell\rangle / N^2 \tag{9}$$

and its variance, or covariance matrix, is given to the same order by the outer product

$$\langle \Delta E \Delta E\rangle = \sum_{k,\ell} (\Phi_k - F)(\Phi_\ell - F)\langle \Delta n_k \Delta n_\ell\rangle / N^2 \quad . \tag{10}$$

The relevant statistical parameters are seen to be only the total mean N and the covariances $\langle \Delta n_k \Delta n_\ell \rangle$ of the reduced counts. Note that the estimator is generally biased, the bias arising from the correlation between the random numerator and denominator of the expression for E. Note also that, since the difference between the total count m_k and the reduced one n_k is not random, their covariances are the same: $\langle \Delta n_k \Delta n_\ell \rangle = \langle \Delta m_k \Delta m_\ell \rangle = \mu_{k\ell}$.

In detail, the mean of the estimated centroid is

$$\langle \underset{\sim}{c} \rangle = \underset{\sim}{s}(1 + \sum_{k,\ell} \mu_{k\ell}/N^2) - \sum_k \underset{\sim}{r}_k (\sum_\ell \mu_{k\ell})/N^2 \qquad (11)$$

and its covariance matrix is

$$\langle \Delta\underset{\sim}{c}\Delta\underset{\sim}{c} \rangle = \sum_{k,\ell} [\underset{\sim}{r}_k \underset{\sim}{r}_\ell - (\underset{\sim}{s}\underset{\sim}{r}_\ell + \underset{\sim}{r}_k \underset{\sim}{s}) + \underset{\sim}{s}\underset{\sim}{s}] \mu_{k\ell}/N^2 \quad . \qquad (12)$$

For the second moment, the mean and the fourth-rank covariance tensor are

$$\langle \underset{\sim}{I} \rangle = \underset{\sim}{M}(1 + \sum_{k,\ell} \mu_{k\ell}/N^2) - \sum_k \underset{\sim}{r}_k \underset{\sim}{r}_k (\sum_\ell \mu_{k\ell})/N^2 \quad , \qquad (13)$$

$$\langle \Delta\underset{\sim}{I}\Delta\underset{\sim}{I} \rangle = \sum_{k,\ell} [\underset{\sim}{r}_k \underset{\sim}{r}_k \underset{\sim}{r}_\ell \underset{\sim}{r}_\ell - (\underset{\sim}{M}\underset{\sim}{r}_\ell \underset{\sim}{r}_\ell + \underset{\sim}{r}_k \underset{\sim}{r}_k \underset{\sim}{M}) + \underset{\sim}{M}\underset{\sim}{M}] \mu_{k\ell}/N^2 \quad , \qquad (14)$$

in which juxtaposed vectors and matrices denote outer products.

The diagonal elements of the detection matrix μ are the variances of the number of photocounts at the detector outputs. Some properties of the variances were discussed in Ref. 5, where Mandel's semiclassical theory of photodetection[13] was applied for several types of laser illumination and target surface roughness. The off-diagonal elements of μ involve correlations of photoelectrons among pairs of detectors in the array. This correlation was demonstrated first by Hanbury Brown and Twiss.[14]

The elements of μ involve fourth-order correlations of the optical field, corresponding to second-order correlations of the irradiance, and are therefore expressible as[15]

$$\mu_{k\ell} = \langle m_k \rangle \delta_{k\ell} + \langle n_k \rangle \langle n_\ell \rangle C^2_{k\ell} \quad , \tag{15}$$

where $\delta_{k\ell}$ is the Kronecker delta and $C_{k\ell}$ is an integrated cross correlation of the instantaneous intensity $I(\underset{\sim}{r},t)$ at the k-th and ℓ-th detectors, at different times t,t':

$$C^2_{k\ell} = \overline{\langle \Delta I_k \Delta I_\ell \rangle} \,/\, \overline{\langle I_k \rangle} \,\overline{\langle I_\ell \rangle} \quad . \tag{16}$$

The overbars denote spatio-temporal averaging over the detector apertures and integration time.

The first term in (15) represents the quantum noise in the count of photons from the image and background radiation and the detector dark current. The other term reflects random fluctuations in the energy W and involves the covariance of the

energy at pairs of detectors. In Ref. 5, C_{kk} was defined as the contrast of the measured fading of the fluctuating irradiance, generalizing the quantity known as contrast of the laser-speckle pattern.

For optical fields that can be modeled as complex Gaussian, weakly stationary processes, $C_{k\ell}^2$ is related to their spatio-temporal degree of coherence by

$$C_{k\ell}^2 = \overline{|\gamma_{k\ell}(t - t')|^2} \quad . \tag{17}$$

For monochromatic illumination and rough targets, for which fluctuations in W are strongest, the image field is such a process, over space. The degree of coherence is then only spatial and is fully determined by the point spread function of the telescope.[5] For the same illumination but targets with smooth surfaces, there are no random fluctuations in energy and the last term in (15) is absent. This term is also zero for temporally noncoherent illumination with coherence time much shorter than the integration time.

4.3 DISCUSSION

To aid in interpreting the general expressions for the performance and accuracy of the estimators, it is useful to relate them to the SNR of the array as a whole. This composite sensor registers a random total reduced count $\sum n_k$ with mean N and variance $\sum \mu_{k\ell}$. The signal-to-noise ratio at the output of the array is

$$R = N/(\sum_{k,\ell} \mu_{k\ell})^{1/2} \quad . \tag{18}$$

The fractional covariances, summing to unity, are

$$\lambda_{k\ell} = \mu_{k\ell}/\sum_{i,j} \mu_{ij} \quad . \tag{19}$$

The correlation between an individual reduced count n_k and the total count, normalized to the overall variance, is

$$\nu_k = \sum_{\ell} \lambda_{k\ell} \quad . \tag{20}$$

The centroid of this fluctuation count is located at

$$\underset{\sim}{q} = \sum_{k} \underset{\sim}{r}_k \nu_k = \sum_{k,\ell} \underset{\sim}{r}_k \lambda_{k\ell} \tag{21}$$

and its second moment is

$$\underset{\sim}{Q} = \sum_{k} \underset{\sim}{r}_k \underset{\sim}{r}_k \nu_k = \sum_{k,\ell} \underset{\sim}{r}_k \underset{\sim}{r}_k \lambda_{k\ell} \quad . \tag{22}$$

In terms of these statistically meaningful quantities, the mean and accuracy of the estimators are expressible by

$$\langle \underset{\sim}{c} \rangle = \underset{\sim}{s} + (\underset{\sim}{s} - \underset{\sim}{q})/R^2 \quad , \tag{23}$$

$$\langle \Delta\underset{\sim}{c}\Delta\underset{\sim}{c} \rangle = \left[\sum_{k,\ell} \underset{\sim}{r}_k \lambda_{k\ell} \underset{\sim}{r}_\ell - \underset{\approx}{q}\underset{\approx}{q} + (\underset{\sim}{s} - \underset{\sim}{q})(\underset{\sim}{s} - \underset{\sim}{q}) \right] / R^2 \quad ; \tag{24}$$

$$\langle \underset{\sim}{I} \rangle = \underset{\sim}{M} + (\underset{\sim}{M} - \underset{\approx}{Q})/R^2 \quad , \tag{25}$$

$$\langle \Delta\underset{\sim}{I}\Delta\underset{\sim}{I} \rangle = \left[\sum_{k,\ell} \underset{\sim}{r}_k \underset{\sim}{r}_k \lambda_{k\ell} \underset{\sim}{r}_\ell \underset{\sim}{r}_\ell - \underset{\approx}{Q}\underset{\approx}{Q} + (\underset{\sim}{M} - \underset{\approx}{Q})(\underset{\sim}{M} - \underset{\approx}{Q}) \right] / R^2 \quad . \tag{26}$$

The rms errors in the estimates are inversely proportional to the overall SNR; the biases are inversely proportional to the square of the SNR.

Equations (23) and (24) can be applied to a tracking system in which the displacement of the image centroid from the optical axis is used to control the monopulse laser radar tracking the TAP. The system can be conceptually similar to typical ones employed for tracking point targets, in which the peak position of the imaging system's point spread function is tracked with a four-quadrant detector.[4] In what follows, these equations are specialized to cases in which the detection matrix μ retains only its diagonal terms.

For monochromatic illumination and optically smooth targets, or for temporally noncoherent illumination and arbitrary target-surface roughness, the off-diagonal terms in μ are absent. Generally, however, the photocounting distribution departs from Poisson statistics, the off-diagonal terms can be present, and the variances of the number of counts at the detector outputs may exceed those given by the Poisson distribution. Specializing to a practically important case of complex Gaussian, weakly stationary random image fields, consider a spatial arrangement of the detectors designed to sample the image plane at the Nyquist rate.[16,17] For well-resolved targets, the spatial bandwidth of the image field is determined by the telescope aperture; sampling at the Nyquist rate implies that the degree of coherence $\gamma_{k\ell}$ in (17) is zero for $k \neq \ell$.

With matrix μ thus rendered diagonal, the reduced count SNR is

$$R = N/(N + N_N + K^2N^2)^{1/2} \quad , \tag{27}$$

where N_N is the total mean noise count and

$$K^2 = \sum \langle n_k \rangle^2 \overline{|\gamma_{kk}|^2}/N^2 \tag{28}$$

is a measure of the bunching of photons, reflecting the fluctuations in the energy W deposited by the image field on the detectors. The mean of the centroid estimator is then

$$\langle \underset{\sim}{c} \rangle = \underset{\sim}{s}(1 + N_N/N^2) + K^2(\underset{\sim}{s} - \underset{\sim}{s}_W) \quad , \tag{29}$$

where $\underset{\sim}{s}_W$ is the centroid of the energy fluctuations $\langle n_k \rangle^2 \overline{|\gamma_{kk}|^2}$. In the absence of the photon-bunching effect, only the first term in (29) remains, and this bias becomes negligible when the signal count N becomes substantial. Even when strong energy fluctuations are present, it should be noted that $\underset{\sim}{s} - \underset{\sim}{s}_W$ is a measure of the nonuniformity of the image irradiance and K^2 is generally less than unity. From (28), one observes that K^{-1} can be interpreted as the SNR at the array output, when it is limited by the laser-speckle noise. This SNR increases as the square root of the number of detectors sensing the image intensity; for Nyquist sampling, this equals the number of degrees of freedom in the image.

The diagonal detection matrix also yields for the covariance matrix of the centroid estimate

$$\langle \Delta\underset{\sim}{c}\Delta\underset{\sim}{c} \rangle = (\underset{\sim}{M} - \underset{\sim}{s}\underset{\sim}{s})/N + (\underset{\sim}{M}_A + \underset{\sim}{s}\underset{\sim}{s})(N_N/N^2) + K^2 [(\underset{\sim}{M}_W - \underset{\sim}{s}_W\underset{\sim}{s}_W) + (\underset{\sim}{s} - \underset{\sim}{s}_W)(\underset{\sim}{s} - \underset{\sim}{s}_W)] , \tag{30}$$

in which $\underset{\sim}{M} - \underset{\sim}{s}\underset{\sim}{s}$ is the image's intrinsic moment of inertia, referred to its own centroid, $\underset{\sim}{M}_W - \underset{\sim}{s}_W\underset{\sim}{s}_W$ is the corresponding moment of the speckle noise, and $\underset{\sim}{M}_A$ that for the array. The geometrical factors depend on image size orientation, and location; they do not change with laser power, provided the illumination is uniform. The coefficients are the inverse — square SNR of the sensor, when limited by the signal shot noise, background and dark current noise, and laser speckle. The last of

these is insensitive to changes in the laser power, while the others can be reduced by increasing the power. For large signals, the laser-speckle noise limits the system's accuracy. For fixed longitudinal geometry of the optical system and given laser coherence, this limitation can be eased by increasing the space-bandwidth product of the imaging system by an increase of the telescope aperture. This not only improves the diffraction-limited resolution of the imaging system, but also produces more degrees of freedom in the image, thereby increasing the speckle-noise-limited SNR.[5] For nonfluctuating targets, the last term in (31) is absent.

The square root of the trace of the matrix $\langle \Delta \underset{\sim}{c} \Delta \underset{\sim}{c} \rangle$, is the rms error in the centroid estimate. Assuming, for simplicity, a uniformly illuminated and reflecting target and cross-spectrally pure light, one has $\underset{\sim}{s}_W = \underset{\sim}{s}$ and $\underset{\sim}{M}_W = \underset{\sim}{M}$. The accuracy of the centroid estimate is then given by

$$\sigma / r_I = \left[K^2 + 1/N + (N_N/N^2)(r_A^2 + s^2)/r_I^2 \right]^{1/2} , \qquad (31)$$

where σ is the standard deviation of the centroid location, r_I and r_A are the optical radii of gyration of the image and array, respectively, and s is the distance of the image centroid from the optical axis. Figure 2 is an asymptotic log-log plot of normalized rms error as a function of signal N. It shows the combined effects of total signal photocounts, background and dark current counts, and laser-speckle noise, as

well as the impact of geometric factors, including image size, centroid displacement, and sensor size. As the signal increases from weak levels, the accuracy is limited first by background light and dark current, and varies with image location. At intermediate signal levels, the image size and the shot noise determine the accuracy. For strong signals, the accuracy becomes independent of signal level, being limited by speckle noise, but still depends on the size of the image.

4.4 CONCLUSIONS

The angular position, shape, and orientation of extended targets can be estimated by use of monopulse laser radars, with target images sensed by a photon counting array. The processing involves conversion of the output counts into measurements of the image centroid and optical moment of inertia.

A Taylor series expansion, valid for small fluctuations of the photocounts about their means, was used to derive the means and covariance matrices of the estimators, to the second order of smallness. It has been found that:

a. Both estimators are biased; the biases are inversely proportional to the square of the overall SNR at the sensor output.

b. The rms errors are inversely proportional to the SNR.

c. The biases and rms errors of the estimators depend on the detection matrix, comprised of the covariances between the photocounts at the outputs of pairs of detectors in the array. The detection matrix becomes diagonal, giving the variances of the photocounts at the individual detector outputs, for either nonfluctuating targets or noncoherent illumination, or also for fluctuating targets generating Gaussian image fields, if the detectors sample them at the Nyquist rate.

d. For diagonal detection matrices and nonfluctuating targets, the bias and rms error of the centroid estimator decrease with increasing laser power; for fluctuating targets they cannot be decreased below the limit imposed by laser-speckle noise. This limitation improves with the number of degrees of freedom in the image, which depends on the diffraction-limited resolution of the imaging system.

4.5 References

1. K. S. Barton, "Radar System Analysis," (Prentice-Hall, Inc., Englewood Cliffs, New Jersey, 1964), pp. 263-315.

2. M. I. Skolnik, "Introduction to Radar Systems," (McGraw-Hill, New York, 1962), pp. 184-189.

3. Ch. McIntyre, W. N. Peters, Ch. Chi and H. F. Wischniea, Proc. of IEEE, 58, pp. 1491-1503, 1970.

4. M. Elbaum, P. Diament, M. King and W. Edelson, "Maximum Angular Accuracy of Pulsed Laser Radar in Photocounting Limit," to be published.

5. M. Elbaum and P. Diament, Appl. Opt. , 15, 2268-2275 (1976)

6. D. L. Snyder, "Random Point Processes," (John Wiley and Sons, New York, London, Sydney, Toronto, 1975), pp. 284-432.

7. J. W. Goodman, Proc. IEEE, 53, 1688-1700, (1965).

8. J. C. Dainty, "Laser Speckle and Related Phenomena," (Springer-Verlag, Berlin, 1975).

9. See the special issue on Speckle in Optics, J. Opt. Soc. Am., No. 11, 66, (1976).

10. G. J. Han and S. S. Shapiro, "Statistical Models in Engineering," (Wiley, New York, 1967), pp. 255-257.

11. L. G. Paratt, "Probability and Experimental Errors in Science," (Dover, New York, 1961), pp. 109-118.

12. This method was used by G. G. Gordon, IEEE Trans. Aerosp. and Electron. Syst., 11, 94-102 (1975), to calculate the mean and variance of the radar cross-section centroid of an ensemble of scatterers.

13. L. Mandel, Proc. Phys. Soc., (London) 74, 233-243 (1959).

14. R. Hanbury Brown and R. Q. Twiss, Nature, London, 177, 27 (1956).

15. J. Pěrina, "Coherence of Light," (Van Nostrand Reinhold Company, New York, 1972), pp. 144-146.

16. M. Schwartz, W. R. Bennett, S. Stein," Communication Systems and Techniques," (McGraw-Hill, New York, 1966), pp. 82-85.

17. A. Rosenfeld and A. C. Kak, "Digital Picture Processing," (Academic Press, New York, San Francisco, London, 1976), pp. 72-75.

4.6 Figure Captions

Fig. 1. Image Plane. I = image, $\vec{r}_k$ = position of k-th detector, m_k = number of photocounts at $\vec{r}_k$, $\vec{c}$ = cetroid estimator, $\langle\vec{c}\rangle$ = mean value of centroid estimator, $\Delta\vec{c} = \vec{c} - \langle\vec{c}\rangle$, and $\vec{s}$ = true image centroid.

Fig. 2. Normalized rms error of $\vec{c}$ vs mean signal counts; asymptotic approximations. The steepest asymptote is background-noise-limited: $\rho_1 = r_I/[N_N(r_A^2 + s^2)]^{1/2}$, $N_1 = (r_A^2 + s^2)N_N/r_I^2$. The middle asymptote is for signal-shot-noise-limited operation: $\rho_2 = K$, $N_2 = K^{-2}$. The horizontal asymptote represents laser-speckle-limited operation.

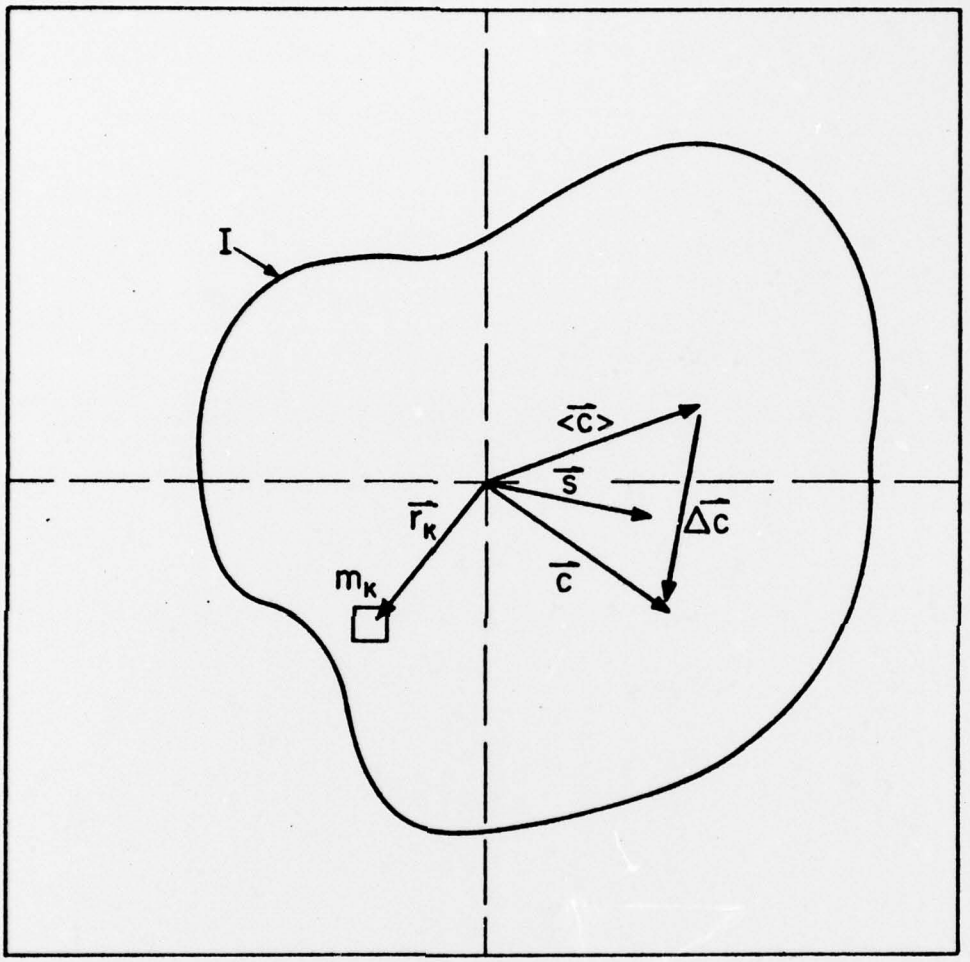

Fig. 1

Fig. 2

SECURITY CLASSIFICATION OF THIS PAGE (When Data Entered)

REPORT DOCUMENTATION PAGE		READ INSTRUCTIONS BEFORE COMPLETING FORM
1. REPORT NUMBER	2. GOVT ACCESSION NO.	3. RECIPIENT'S CATALOG NUMBER
4. TITLE (and Subtitle) Photocounting Image Tracking of Fluctuating Targets		5. TYPE OF REPORT & PERIOD COVERED Technical Report
		6. PERFORMING ORG. REPORT NUMBER T1/364-3-65
7. AUTHOR(s) Marek Elbaum		8. CONTRACT OR GRANT NUMBER(s) DAAK40-76-C-0500
9. PERFORMING ORGANIZATION NAME AND ADDRESS Riverside Research Institute 80 West End Avenue New York, N.Y. 10023		10. PROGRAM ELEMENT, PROJECT, TASK AREA & WORK UNIT NUMBERS ARPA Order 2281, Amd.14 Tech. RQMT 6004 Par. 3.4
11. CONTROLLING OFFICE NAME AND ADDRESS MIRADCOM Redstone Arsenal, Alabama 35809		12. REPORT DATE February 1977
		13. NUMBER OF PAGES 116 + vi
14. MONITORING AGENCY NAME & ADDRESS(if different from Controlling Office)		15. SECURITY CLASS. (of this report) UNCLASSIFIED
		15a. DECLASSIFICATION/DOWNGRADING SCHEDULE

16. DISTRIBUTION STATEMENT (of this Report)

17. DISTRIBUTION STATEMENT (of the abstract entered in Block 20, if different from Report)

Unlimited Distribution

18. SUPPLEMENTARY NOTES

19. KEY WORDS (Continue on reverse side if necessary and identify by block number)

Laser Radar	Laser Speckle
Position Estimation	Photocounting
Tracking	Noncoherent Detection

20. ABSTRACT (Continue on reverse side if necessary and identify by block number)

A theory of estimation of angular position and other attributes of optically rough and smooth targets with a monopulse laser radar is developed. It applies to systems deriving information about the target position by sensing its image with an array of noncoherent detectors. The theory develops quantitative formulations of the fundamental limitations imposed upon measurement accuracy by the shot noise arising from both

DD FORM 1 JAN 73 1473 EDITION OF 1 NOV 65 IS OBSOLETE

SECURITY CLASSIFICATION OF THIS PAGE (When Data Entered)

the target return and the background radiation, by the detector dark current, and by the random fluctuations of the target cross section.